In situ XAS study on the Cu and Ce local structural changes in a CuO–CeO/AlO catalyst under propane reduction and re-oxidation

Geert Silversmit, Hilde Poelman, Veerle Balcaen, Philippe M. Heynderickx, Maria Olea, Sergey Nikitenko, Wim Bras, Philippe F. Smet, Dirk Poelman, Roger de Gryse, et al.

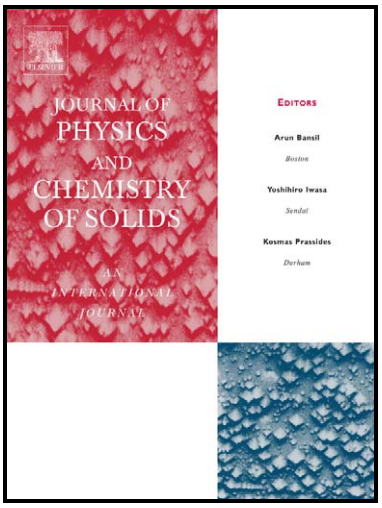

www.elsevier.com/locate/jpcs

In situ XAS study on the Cu and Ce local structural changes in a $CuO–CeO_2/Al_2O_3$ catalyst under propane reduction and re-oxidation

Geert Silversmit, Hilde Poelman, Veerle Balcaen, Philippe M. Heynderickx, Maria Olea, Sergey Nikitenko, Wim Bras, Philippe F. Smet, Dirk Poelman, Roger De Gryse, Marie-Françoise Reniers, Guy B. Marin

PII: S0022-3697(09)00171-1
DOI: doi:10.1016/j.jpcs.2009.07.008
Reference: PCS 5898

To appear in: *Journal of Physics and Chemistry of Solids*

Received date: 17 March 2009
Revised date: 28 May 2009
Accepted date: 8 July 2009

Cite this article as: Geert Silversmit, Hilde Poelman, Veerle Balcaen, Philippe M. Heynderickx, Maria Olea, Sergey Nikitenko, Wim Bras, Philippe F. Smet, Dirk Poelman, Roger De Gryse, Marie-Françoise Reniers and Guy B. Marin, In situ XAS study on the Cu and Ce local structural changes in a $CuO–CeO_2/Al_2O_3$ catalyst under propane reduction and re-oxidation, *Journal of Physics and Chemistry of Solids*, doi:10.1016/j.jpcs.2009.07.008

In situ XAS study on the Cu and Ce local structural changes in a $CuO-CeO_2/Al_2O_3$ catalyst under propane reduction and re-oxidation

Geert Silversmit[1,*], Hilde Poelman[1], Veerle Balcaen[2], Philippe M. Heynderickx[2], Maria Olea[2], Sergey Nikitenko[3], Wim Bras[3], Philippe F. Smet[1], Dirk Poelman[1], Roger De Gryse[1], Marie-Françoise Reniers[2] and Guy B. Marin[2]

[1] *Ghent University, Department of Solid State Sciences, Krijgslaan 281 S1, B-9000 Gent, Belgium*
[2] *Ghent University, Laboratorium voor Petrochemische Techniek, Krijgslaan 281 S5, B-9000 Gent, Belgium*
[3] *Netherlands Organisation for Scientific Research (NWO), DUBBLE @ ESRF, BP 220, 38043 Grenoble CEDEX 9, France*

Abstract

The redox behaviour of a $CuO-CeO_2/Al_2O_3$ catalyst is studied under propane reduction and re-oxidation. The evolution of the local Cu and Ce structure is studied with in-situ transmission X-ray absorption spectroscopy (XAS) at the Cu K and Ce L_3 absorption edges.

CuO and CeO_2 structures are present in the catalyst as such. No structural effect on the local Cu structure is observed upon heating in He up to 873 K or after pre-oxidation at 423 K.

Exposure to propane at reaction temperature (600-763 K) fully reduces the Cu^{2+} cations towards metallic Cu^0. Quick EXAFS spectra taken during reduction show a small amount of intermediate Cu^{1+} species. Parallel to the CuO reduction, CeO_2 is also reduced in the same temperature range. About 25 % of the Ce^{4+} reduces rapidly to Ce^{3+} in the 610-640 K temperature interval, while beyond 640 K a further slower reduction of Ce^{4+} to Ce^{3+} occurs. At 763 K, Ce reduction is still incomplete with 32 % of Ce^{3+}.

Re-oxidation of Cu and Ce is fast and brings back the original oxides.

The propane reduction of the $CuO-CeO_2/Al_2O_3$ catalyst involves both CuO and CeO_2 reduction at similar temperatures, which is ascribed to an interaction between the two compounds.

Keywords: A. oxides, C. XAFS (EXAFS and XANES), D. electronic structure, D. microstructure

* Corresponding author, Geert.Silvermit@UGent.be
Present address: X-ray Microspectroscopy and Imaging Research Group (XMI), Department of Analytical Chemistry, Ghent University, Krijgslaan 281 S12, B-9000 Gent, Belgium

1. Introduction

Transition metal based catalysts are frequently applied as substitute for the more expensive noble metal catalysts. Supported copper oxide has received considerable attention in this respect, as it is one of the most active and selective catalysts for various reactions: steam reforming of methanol [1], water gas shift reaction [2], reduction of NO_x and SO_2 [3]. Furthermore, supported CuO has been successfully applied in CO and CH_4 oxidation reactions, making it a candidate for VOC (volatile organic compound) emission control [4]. The properties of supported CuO catalysts can be enhanced by addition of yet another oxide to the support. For this purpose, the properties of CeO_2 are to be noted because of its enhancement of CuO activity and stabilising effect against sintering [5-7].

In view of application as total oxidation catalyst for elimination of light alkanes, the structural changes of a CuO-CeO_2/Al_2O_3 commercial catalyst under propane reduction and reoxidation have been studied in the temperature range 600-763 K. Reduction of CuO can either follow a one-step $Cu^{2+} \rightarrow Cu^0$ mechanism or rather proceed through an intermediate Cu^{1+} state. The presence of an intermediate Cu^{1+} state depends on the conditions of reduction such as gas flow rate and temperature ramping speed [8-9]. In studies on supported copper oxide, Cu_2O has equally been observed as an intermediate phase, e.g. with ex situ XRD [10] or through analysis of XAFS data identifying Cu^{1+} during reduction [9-13]. In literature, the addition of CeO_2 to the catalyst is held responsible for an enhanced reducibility of CuO [6-7, 14]. Hence, for a complete picture of the catalyst's redox properties, a study of structural changes under redox conditions must include both CuO and CeO_2 compounds. In this way, the specific contribution of each compound to the reaction can be separated and evaluated. In situ XAS presents the ideal tool for this purpose, as it is element specific and applicable under reaction conditions.

In this work, the redox properties of the CuO-CeO_2/Al_2O_3 catalyst were investigated using quick X-ray absorption spectroscopy (Q-XANES and Q-EXAFS). With appropriate choice of redox conditions, this technique allows following the catalyst under reaction, yielding the structural and electronic properties of Cu and Ce during in-situ propane reduction and re-oxidation. After a preliminary analysis of the Cu environment in the CuO-CeO_2/Al_2O_3 catalyst [15], a detailed XAS analysis of the changes at both the Cu K and Ce L_3 edge is now presented. In this way, intermediate

states and contribution of each specific compound to the structural changes of the catalyst are identified.

2. Experimental

2.1. Catalyst characterisation

The CuO-CeO_2/Al_2O_3 catalyst was synthesized via impregnation of γ-Al_2O_3 with $Cu(NO_3)_2$ and $Ce(NO_3)_4$ precursors, pressed into extrudates, dried and calcined above 723 K. The latter material was crushed to fine powder (< 20 μm) for XAS experiments and characterisation.

X-ray diffraction (XRD) measurements were performed with a Siemens Diffractometer Kristalloflex D5000, using Cu Kα radiation. The catalyst material as received presented broad lines from ceria and alumina, and narrow diffraction peaks for CuO (Figure 1, A). The XRD pattern of a sample used in a XAS propane reduction showed very sharp Cu diffraction lines instead of the original CuO lines (Figure 1, B). Estimates of the crystallite size of the different particles for both samples were obtained from the width of the diffraction peaks using Scherrer's equation [16]. In the fresh sample, CuO is mainly present as large crystallites, whereas both the alumina and ceria are smaller sized crystallites, a few nm large (Table 1). Within experimental error, no significant difference could be found between different peaks from one compound. Hence, it is concluded that the crystallites are essentially isotropic. The sharp CuO and Cu diffraction lines point towards crystallites of some 100 nm in size, i.e. an order of magnitude larger than the alumina and ceria. As the width of these CuO and Cu peaks lies close to the instrumental width, small differences in FWHM can lead to large variation in resulting size and hence, accurate crystallite size determination is impossible. Therefore, an order of magnitude is indicated in table 1 for CuO and Cu crystallite sizes, while for the other compounds, values averaged over different diffraction lines are given.

HRTEM (High Resolution Transmission Electron Microscopy) analysis of the catalyst was performed with a JEM-2200FS instrument (JEOL, 200 keV with scanning unit and EDX). Figure 2 shows the STEM images and corresponding elemental mappings for Cu K, Ce L and Al K fluorescence radiation on the CuO-CeO_2/Al_2O_3 catalyst. The left image (Figure 2, A) presents a large CuO feature in an Al_2O_3 matrix, and no Ce intensity. The CuO entity displays sharp edges and measures at least 100 nm

square. In the right image (Figure 2, B), a cluster of ceria particles about 100 nm wide is visible within the alumina matrix. No Cu intensity was registered in this image. Similar images were observed throughout the catalyst sample. Performing selective area diffraction (SAD) upon this sample, the crystallinity of the different compounds was determined (Figure 3). The alumina matrix of the catalyst gives rise to rings of diffraction in the SAD pattern (Figure 3, A), indicating randomly oriented nanoparticles. The distances between the rings correspond with gamma-alumina. Focussing on a ceria cluster, rings from the alumina matrix are accompanied by ring fragments arising from ceria nanoparticles (Figure 3, B). The distances agree with crystalline CeO_2. As the rings from ceria are not complete, it seems that there is a partial preferential orientation, aligning the particles within about 20° around the <110> direction in this case. Finally, SAD on a CuO entity yields sharp diffraction spots, corresponding to a large single crystal particle. Hence, the XRD findings are largely confirmed by the present TEM results: the CuO-CeO_2/Al_2O_3 catalyst consists mainly of large CuO blocks and clustered CeO_2 nanoparticles embedded in a matrix of nanocrystalline Al_2O_3.

Table 2 contains general characteristics of the CuO-CeO_2/Al_2O_3 catalyst. The specific surface area of the catalyst was determined with a Micromeritics ASAP 2010 instrument with N_2 adsorption at 77 K. Full elemental composition of the catalyst was obtained using inductively coupled plasma (ICP-MS) analysis (IRIS Advantage system, Thermo Jarrell Ash) by fusion in NaO and NaOH. All samples were dried at 378 K before mineralization. The catalyst contains 9.3 wt% Cu and 5.2 wt% Ce, corresponding to 9.17 µmol Cu/m^2 and 2.35 µmol Ce/m^2 respectively. Larsson et al. have investigated a series of CuO catalysts supported on ceria modified alumina [5]. They found CuO diffraction peaks for catalysts containing at least 6 µmol Cu/m^2. Hence, the given loading of 9.17 µmol Cu/m^2 is high enough to give rise to bulk CuO and thus also to CuO crystallites.

Surface atomic concentrations were obtained by means of XPS using a Perkin Elmer PHI ESCA 5500 system equipped with a monochromatic 450 Watt Al Kα source. The crushed CuO-CeO_2/Al_2O_3 catalyst gave rise to a Cu/Al XPS intensity ratio of 0.12 (see Table 2). The overall Ce 3d signal was very weak and allowed no further analysis (not shown). The Cu 2p photoline displayed a satellite feature at higher binding energy, characteristic for Cu^{2+}, with a Cu_{sat}/Cu_{main} ratio of 0.28 (not shown; see Table 2). As Cu^{1+} is known not to exhibit such feature, the Cu_{sat}/Cu_{main} intensity ratio can be used to

evaluate the presence of reduced copper. The value found here is lower than the literature values of ~0.5 for bulk CuO [4, 6, 12]. Hence, this could point towards the presence of some reduced copper, possibly caused by photoreduction of CuO in the process of the XPS measurement.

2.2. X-ray absorption measurements

The copper K-edge and cerium L_3-edge X-ray absorption spectra were recorded in transmission mode at the DUBBLE beamline (Dutch-Belgian beamline, BM26A) [17] of the 6 GeV ESRF synchrotron (Grenoble, France) during a uniform filling mode, giving a typical storage ring current of 200 down to 160 mA within one synchrotron run. The synchrotron radiation emitted by the bending magnet (magnetic field strength: 0.4 Tesla) was monochromatized with a double crystal Si(111) monochromator. The higher harmonics of the primary energy that are also being transmitted by the monochromator were suppressed with the mirror after the monochromator. Ionisation chambers filled with Ar/He mixtures at atmospheric pressure were used to measure the intensity of the incoming, I_0, and transmitted, I_t, X-ray beam. A reference sample placed between the second and the third ionisation chamber is used for energy scale correction, especially during the QEXAFS mode.

The samples were pressed into self-supporting pellets in the rectangular shaped hole of a stainless steel sample holder. The pellet thickness was chosen to give an absorption jump of about 1.0 over the Cu K or Ce L_3 absorption edges. In a typical sample preparation, 43 mg of catalyst powder was mixed and pressed with about 12 mg of BN, an inert and weakly absorbing binder, for the Cu K-edge spectra while 50 mg of pure catalyst powder was used for the Ce L_3-edge spectra.

The in-situ X-ray absorption spectroscopy (XAS) measurements were performed in a stainless steel XAS chemical reactor cell (volume ~ 1.75 l) designed and built at the department of Solid State Sciences at the Ghent University. Kapton foils (25 µm thickness) were used as X-ray transparent windows. The cell has a double wall design, allowing a cooling water flow and preventing the heating of the Kapton windows. The sample holder with pressed pellet was mounted inside the reactor in an inconel block with thermocoax wiring for resistive heating allowing a maximum sample holder temperature of 973 K. The sample holder temperature was controlled with an Eurotherm

PID temperature control. A gas flow through the reactor was established using mass flow controllers. The design resembles that of a pellet cell with gas flow streaming on both sides of the pellet [18].

Reduction treatments were performed with propane gas flows diluted in He (2.2 or 10% propane in He), and re-oxidation treatments with O_2 flows in He (50%) at atmospheric pressure. Specific temperatures and gas flow rates are given below. The catalyst reduction was followed in-situ by recording full EXAFS scans in 1 minute in a quick scanning EXAFS mode (Q-EXAFS). The fast scans resulted in high quality Cu K EXAFS spectra. Although good Ce L_3 XANES spectra were obtained in the quick scanning mode, the data quality did not allow to extract acceptable Ce L_3 EXAFS signals.

The XAS spectra of Cu foil, Cu_2O, CuO, Ce, CeF_3 and CeO_2 powders were recorded in transmission mode at ambient temperature and pressure as references. The energy scale for the Cu K-edge absorption spectra was calibrated to the first maximum of the first derivative spectrum of a metallic Cu foil measured simultaneously with the samples by using the second and third ionisation chamber at ambient conditions. For the Ce L_3 spectra there was insufficient flux left to measure a reference spectrum in between the second and third ionisation chamber. Therefore a glitch in the I_0 signal around 5987.46 eV was used to correct the energy scale during the Q-EXAFS scanning mode.

2.3. EXAFS data analysis and fit parameter errors

The EXAFS data reduction and analysis were performed with the XDAP software [19]. The pre-edge background was subtracted using a modified Victoreen curve [20] and the atomic background, μ_0, was subtracted with a cubic spline routine [21]. The pre-edge background subtracted spectra were normalised to the edge jump, which was taken to the value of the atomic background at 50 eV above the edge position. The fit parameters were determined by multiple shell fitting in R-space, by applying the difference file technique using Fourier Transformations [22]. The agreement between model and fit in *R* or *k*-space is expressed by a variance, which gives the relative deviation between model and experiment in percentages [20]. Phase shift and backscattering amplitude functions used to calculate the Cu-Cu and Cu-O contribution

in an EXAFS spectrum were obtained with FEFF 8.0 calculations [23] on fcc Cu metal and Cu_2O spherical clusters with a radius of 8.0 Å and 8.2 Å respectively.

In order to quantify the error upon the EXAFS analysis and fits, both systematic and statistical errors should be taken into account. As recommended in the report of the International Workshop on Standards and Criteria in X-ray Absorption Spectroscopy [24] by the International X-Ray Society, an estimate of the systematic errors in the EXAFS analysis and data reduction can be obtained by using the calculated Cu-Cu and Cu-O phase and amplitude functions to fit the experimental spectra of different references with known structure and treating them as 'unknown' samples. The differences between the fit results and the crystal structures serve as an estimate of the systematic errors. Four reference measurements were available for the systematic errors evaluation: Cu metal foil and Cu_2O powder measured at 12 K and at ambient conditions. The following procedure was used to estimate these systematic errors.

As a first step, the first shell in Cu foil (Cu-Cu) and Cu_2O (Cu-O) are fitted with the calculated phase shift and backscattering amplitude functions. The S_0^2 factor for the Cu-Cu and Cu-O contribution was tuned to have agreement with the co-ordination number of the first Cu-Cu shell in Cu metal (R = 2.556 Å, N = 12) and the first Cu-O shell in Cu_2O (R = 1.849 Å, N = 2) [25], both for the spectra taken at 12 K and under ambient conditions. The resulting S_0^2 values for the Cu metal and the Cu_2O spectrum taken at 12 K were 0.89 and 0.73 respectively, comparable with the values reported in [25] for the same structures measured at 83 K. The resulting S_0^2 factors for the spectra taken at ambient conditions were 0.86 and 0.80 for the Cu-Cu and Cu-O contributions respectively.

As a second step, new fits using up to 3 shells for the Cu foil and 2 shells for the Cu_2O structures (both spectra recorded at 12 K and ambient conditions) were performed in order to treat these reference spectra as 'unknown' samples. The Debye-Waller factors over Cu shells in the Cu foil fit were constrained to one optimised value. The maximum absolute differences between the crystal structure and the fit values over different k-weightings (k^1, k^2 and k^3) and over the four spectra are taken as systematic error values and are summarized in Table 3. For the systematic error on the Debye-Waller factor (σ^2) we take 10%, a typical value found for the amplitude factors from theoretical references [25]. The errors calculated from the statistical error in the data were smaller than 10% of the systematic errors and can therefore be neglected.

The nearest neighbours for Cu in CuO are two O shells at bond distances of 1.951 and 1.961 Å, both with a co-ordination number of 2. Using the optimized theoretical Cu-Cu and Cu-O amplitude and phase functions, a fit of the CuO EXAFS spectrum taken at ambient conditions with the crystallographic co-ordination numbers was possible, but large absolute ΔE_0 values were needed for the Cu-O shells compared to the Cu_2O fits. A fit with acceptable ΔE_0 values was possible by combining the two nearest Cu-O shells into one single Cu-O shell with a co-ordination number of 4, using a S_0^2 of 0.63.

An EXAFS fit can be considered to be proper if it yields a good result in different *k*-weightings (k^1, k^2 and k^3). Therefore, EXAFS fits were performed with a k^1, k^2 and k^3 weighting and the reported fit parameters are the average values. The standard deviation over the values is added to the systematic errors to obtain the total error: $Err_{tot} = Err_{\text{systematic}} + \sigma_{\text{kweightings}}$. The k^1 weighted fits on Cu_2O and Cu metal taken at ambient conditions resulted in co-ordination numbers for the first Cu shell in the Cu_2O and the higher shells in Cu metal that were considerably larger than the crystal structure values (up to 40 %), while the corresponding co-ordination numbers obtained from the k^2 and k^3 weighted fits only deviated by maximum 10%. Reported co-ordination numbers for these Cu contributions are therefore the average over the k^2 and k^3 weighted fits only.

3. Results and discussion

3.1. Local Cu structure

3.1.1. Local Cu structure at ambient conditions

The Cu K XANES spectrum for the as prepared catalyst recorded in He at ambient temperature is compared in Figure 4 with the spectra of Cu metal, Cu_2O and CuO references taken at ambient conditions. The good resemblance with the CuO XANES indicates that at ambient temperature the local structure in the catalyst is as in CuO. However, the catalyst has a more intense white line (first peak after the absorption edge), indicating a higher $4p_\sigma$ density of states compared to the bulk CuO crystal structure. The local CuO structure in the catalyst is further supported by the good agreement between the k^2-weighted EXAFS signals and corresponding Fourier Transforms for the catalyst and the CuO reference as shown in Figure 5. The intensity in the k^2-weighted Fourier Transform for the Cu-O shell (0.0-2.0 Å) is more intense for

the catalyst than for the CuO reference, while the intensity for the Cu-Cu shells (2.0-3.0 Å) is lower. An EXAFS fit with the parameters from the CuO structure as starting values was possible, see Figure 6 and Table 4 for the optimised parameters. Compared to the CuO crystal structure, similar bond distances are obtained, but a higher total Cu-O co-ordination number is found, 5.8 (± 0.4) instead of 4, and a lower total Cu-Cu co-ordination number, 3.3 (±1.5) instead of 8.

For CuO/Al_2O_3, different species are reported depending on copper loading and calcination temperature [4, 26]. If the calcination temperature is high enough (> 973 K), bulk $CuAl_2O_4$ can form through solid-solid interaction between CuO and Al_2O_3 [27]. For lower calcination temperatures and low loadings of Cu, < 8-10 wt%, well-dispersed isolated Cu^{2+} has been observed, as well as a copper surface spinel [4, 26]. The latter is a defective $CuAl_2O_4$-like species, with Cu^{2+} occupying a distorted octahedral geometry in the alumina surface [28]. With increasing copper loading, > 8-10 wt%, bulk CuO starts to appear, giving rise to XRD diffraction peaks [4, 26, 29]. If ceria is added to the alumina, the threshold between well-dispersed and bulk CuO still holds for low ceria loadings [5, 29]. At very high ceria loadings, ~ 25 wt%, CuO is no longer found in crystalline form but rather appears surface dispersed on both alumina and ceria, even for high Cu loadings [29].

For the present system, XRD gives no indication of bulk copper aluminate being formed, the calcination temperature being too low. The diffraction peaks for CuO as well as the TEM images clearly show that the Cu loading in this CuO-CeO_2/Al_2O_3 catalyst gives rise to bulk CuO crystallites (see Table 1, Figure 2, A and Figure 3, C). The good EXAFS fit obtained starting from the CuO structure is in accordance with the CuO species identification for this catalyst. Further, the Cu-Cu contributions around 3 Å show that the copper oxide has indeed neighbouring CuO in the catalyst. Moreover, the satisfactory fit leaves no indication of a significant amount of Cu_2O present in the catalyst sample in ambient conditions. Hence, the lower Cu_{sat}/Cu_{main} ratio of 0.28 as found with XPS (§ 2.1) can be ascribed to photoreduction during the XPS measurements rather than to the intrinsic presence of reduced copper oxide.

3.1.2. Local Cu structure after drying, pre-oxidation and C_3H_8 adsorption

The local structure of a catalyst may be altered by pre-treatments given to it like drying, pre-oxidation, adsorption of reactants below reaction temperature, … . No

changes could be observed in the Cu K XANES spectra for the catalyst after drying up to 423 K in a He flow of 7.4×10^{-5} mol/s (at standard temperature and pressure), after a pre-oxidation at 423 K in a O_2 flow of 3.7×10^{-5} mol/s in 3.7×10^{-5} mol/s He and after pre-adsorption with C_3H_8 at 473 K in a C_3H_8 flow of 7.4×10^{-6} mol/s in 6.7×10^{-5} mol/s He. Moreover the EXAFS analysis for these pre-treatment spectra resulted in fit parameters similar to the values for the catalyst recorded at ambient temperature in He. Hence, the above mentioned pre-treatments do not influence the local Cu structure. Further drying under He flow of the as prepared catalyst up to 873 K does not alter the XAS spectra either (spectra not shown).

3.1.3. Local Cu structure after reduction with C_3H_8

The XANES, $k^2*\chi(k)$ and FT[$k^2*\chi(k)$] spectra for the catalyst after reduction with propane at a reaction temperature of 723 K in a propane flow of 7.4×10^{-6} mol/s in 6.7×10^{-5}mol/s He at ambient pressure are given in Figure 7. A clear metallic Cu spectrum is present, indicating that complete reduction took place. The Cu K EXAFS fit result is given in Figure 8 and Table 5, the nearest Cu-Cu bond distance is somewhat smaller than the bond distance for the crystal structure of metallic fcc Cu.

3.1.4. Reversibility of the reduction/oxidation process

After an initial drying period of 2 hours in a He flow of 1×10^{-3} mol/s at 423 K, four propane reductions and three intermediate re-oxidations were performed consecutively on the CuO-CeO_2/Al_2O_3 catalyst. The reduction and re-oxidation treatments were carried out at 698 K in respectively a propane flow of 7.4×10^{-6} mol/s in 6.7×10^{-5} mol/s He and an O_2 flow of 3.7×10^{-5} mol/s in 3.7×10^{-5} mol/s He. A metallic Cu structure develops after each reduction and each re-oxidation restores the CuO structure as is present at ambient conditions, indicating a reversible local Cu structure in the catalyst (spectra not shown).

346 *3.1.5. Evolution of the local Cu structure during isothermal C_3H_8 reduction*

347 The evolution of the local Cu structure in the CuO-CeO_2/Al_2O_3 catalyst during
348 reduction with propane was followed by recording full XAS spectra in a measuring time
349 of 1 minute. The reduction was performed at a reaction temperature of 623 K in a
350 propane flow of 7.4×10^{-6} mol/s in 3.4×10^{-4} mol/s He at ambient pressure. The catalyst
351 was pre-treated by flushing with C_3H_8/He for 15 minutes at 424 K, followed by a fast
352 heating to the reaction temperature of 623 K. The acquisition of the XAS spectra was
353 already started during the heating and reaction temperature was reached after 3 minutes.
354 The corresponding Cu K-edge QXANES spectra are given in Figure 9. Effect of the
355 reduction on the XANES spectra can already be seen from the very beginning of the
356 heating, before the reaction temperature was reached, as appears from the decreasing
357 intensity in the $4p_\sigma$ transition just after the edge. Although the post-edge structure can
358 be seen as a linear combination of the first ($Cu^{2+}O$) and last (Cu^0) spectrum, the edge
359 structure cannot. During the reduction process, a shoulder appears on the lower half of
360 the absorption edge which moves to lower energy values. A small pre-edge peak starts
361 to develop from this shoulder, but then this pre-edge peak evolution stops and
362 disappears again, see the inset in Figure 9. This implies that the XANES spectra cannot
363 solely be regarded as a linear combination of the first ($Cu^{2+}O$) and last (Cu^0) spectrum.
364 As the Cu_2O structure has a large pre-edge peak, see Figure 4, the observed pre-edge
365 development can be ascribed to the presence of some Cu_2O during the propane
366 reduction process.

367 The corresponding QEXAFS spectra are also given in Figure 9. Following the
368 evolution of the XANES spectra, a linear combination fit with three base components
369 (one for each Cu oxidation state) was performed on this QEXAFS spectrum series. As
370 Cu^{2+} component in the linear combination fit, a fully oxidized spectrum (i.e. at the
371 beginning of the reduction series) was used, a fully reduced spectrum (i.e. at the series'
372 end) was taken as Cu^0 component and the Cu_2O reference spectrum was chosen as Cu^{1+}
373 component. The resulting percentages of each component as a function of time in the
374 reduction process are given in Figure 10. The exact fit percentages are dependent on the
375 amplitude of the base spectra. As the reference Cu_2O spectrum was taken at ambient
376 temperature from a Cu_2O reference powder, presenting a different disorder than present
377 in the catalyst, the scaling factor for the Cu_2O contribution is not known. Hence, the
378 reported concentrations are only qualitative and not quantitative. The Cu_2O spectrum is

found as a minor intermediate component, which has a maximum after about 6 minutes reduction time.

The evolution of the XANES and EXAFS spectra (Figure 9) clearly shows the presence of an intermediate Cu^{1+} phase upon propane reduction at 623 K over the $CuO-CeO_2/Al_2O_3$ catalyst. Caballero et al. investigated a CuO/ZrO_2 catalyst under C_3H_8 diluted in He at 773 K [12]. Under these conditions, reduction of the catalyst was incomplete and factor analysis of the XANES spectra identified three components: CuO, Cu_2O and Cu. In methanol steam reforming over CuO/ZrO_2, Cu_2O was obtained as post-reaction oxidation state for certain Cu loadings and water/methanol ratios [10]. H_2 reduction of the same catalyst confirmed the presence of the Cu^+, now as intermediate towards metallic Cu [10]. In H_2 reduction or oxidative methanol reforming over CuO/ZnO_2 [30-31] and in $CO-CO_2-H_2/Ar$ reduction of a $CuO/ZnO_2/Al_2O_3$ catalyst, Cu_2O was equally identified as an intermediate copper phase preceding the formation of metallic Cu [11]. But the presence of Cu_2O as intermediate during reduction of CuO is not general: CuO in ZSM5 was found to reduce in H_2-TPR via Cu_2O in small CuO particles only, while the larger ones exhibited a direct $Cu^{2+} \rightarrow Cu^0$ transition [13]. For unsupported CuO, it was found that the presence of an intermediate Cu_2O phase upon CO or H_2 reduction strongly depends on the reduction conditions and the reduction can follow either a direct or a two-step transition [8-9]. The sequential pathway is observed when either a limited feed or fast temperature ramping conditions are applied, i.e. a more 'mild' reduction, where Cu_2O can appear.

Hence, the presence of Cu^{1+} in present $CuO-CeO_2/Al_2O_3$ catalyst during the propane reduction process is not surprising but related to the CuO particle structure and conditions of reduction. Under a flow of 7.4×10^{-6} mol/s propane in 3.4×10^{-4} mol/s He at ambient pressure and 623 K, the large CuO crystallites of the catalyst are reduced through a Cu^{1+} intermediate state. These conditions are hence 'mild' enough to allow the Cu_2O intermediate state to occur during reduction.

3.2. Local Ce structure

3.2.1. Local Ce structure at ambient conditions

The Ce L_3 XANES spectra for Ce^{3+} compounds have a strong absorption line at the absorption edge (white line: WL) due to a $2p_{3/2} \rightarrow (4f^1)5d^*$ electronic transition (d^*

412 denotes an excited electron in the d orbital). Ce^{4+} compounds however present a double
413 white line. These two peaks correspond to the $2p_{3/2} \rightarrow (4f^1\underline{L})5d^*$ and $2p_{3/2} \rightarrow (4f^0)5d^*$
414 transitions ($\underline{L}$ denotes that an electron from an O2p orbital is transferred to a Ce4f
415 orbital) [32-35]. The Ce L_3 spectra for CeO_2, CeF_3 and Ce powder are given in
416 Figure 11 as references, while more spectra of Ce^{3+} and Ce^{4+} compounds can be found
417 in for example [36].
418 The Ce L_3 XANES spectrum for the CuO-CeO_2/Al_2O_3 catalyst at ambient
419 conditions is compared with the references in Figure 11. A local CeO_2 structure can be
420 concluded for the CuO-CeO_2/Al_2O_3 catalyst at ambient conditions, with Ce^{4+} oxidation
421 state.
422 When ceria is supported on alumina, up to 3 different Ce species have been
423 identified in literature [37]: Ce species in Al_2O_3 cation vacancies (named a $CeAlO_3$
424 precursor phase, with Ce^{3+} oxidation state), well-dispersed small CeO_2 particles, too
425 small to be detected in XRD, and bulk-like CeO_2. In the present CuO-CeO_2/Al_2O_3
426 catalyst, the ceria loading of 2.35 μmol Ce/m^2 was in the XRD analysis identified as
427 ceria particles of size around 6 nm (see Table 1), while TEM showed them to be
428 clustered within the alumina matrix (Figure 2B). At ambient conditions the observed Ce
429 oxidation state is 4+ (Figure 11). Hence, it is concluded that Ce is present as CeO_2
430 particles only and not as $CeAlO_3$ precursor state, which bears a Ce^{3+} state.
431
432
433 *3.2.2. Local Ce structure after C_3H_8 reduction and re-oxidation*
434 Two subsequent reductions (RED1 and RED2) were performed on the CuO-
435 CeO_2/Al_2O_3 catalyst, with a re-oxidation in between. The sample was heated from 600
436 to 763 K (723 K for RED2) in steps of 8 K in a propane flow of 7.4×10^{-6} mol/s in
437 3.4×10^{-4} mol/s He at ambient pressure. The final Ce L_3 spectra for each reduction and
438 the intermediate re-oxidation (performed at 763 K, in an O_2 flow of 7.4×10^{-6} mol/s in
439 3.4×10^{-4} mol/s He at ambient pressure) are shown in Figure 12. The two reductions
440 yield a similar spectrum. The re-oxidation brings back the CeO_2 structure. Compared to
441 the oxidized spectrum, the main edges in the spectra for the reduction treatments are
442 shifted to lower X-ray energy values and there is a different ratio in the intensity of the
443 two white lines. As two white lines can still be noticed after reduction, Ce^{4+} cations are
444 still present. In order to quantify the amount of Ce^{3+} in the spectra upon the reduction

treatments, a fit of the Ce L_3 XANES was performed with the CeO_2 XANES spectrum as model for the Ce^{4+} oxidation state and the CeF_3 spectrum for the Ce^{3+} oxidation state. The fit procedure used is explained below.

Ce L_3 XANES spectra are commonly analysed by fitting procedures in which the white line transitions are approximated with Lorentzian curves and the absorption step by an arctangent function [32, 35-36, 38]. The resulting fits on the CeF_3 and CeO_2 references are given in Figure 13. For the CeF_3 reference compound spectrum for example, the fit function was $\frac{a}{\pi} * \left(\arctan\left(E-b\right)+\pi/2\right)+c*\left(1+\left(2*\left(E-d\right)/e\right)^2\right)^{-1}$, with *E* the X-ray energy value. The first term represents an arctangent with *a* and *b* the height and position of its inflection point respectively, while the second term is a Lorentzian function with *c*, *d* and *e* its height, position and width at half maximum respectively. For the CeO_2, three Lorentzians are needed, one for each WL and an extra component at the rising edge. This third component is in literature often ascribed to some Ce^{3+} present in the CeO_2 [35], but more recently attributed to many-body final states of the 2p→5d transition [34]. According to this last reference, we have considered this third component as an intrinsic feature of the CeO_2 XANES spectra.

Relative constraints on the height, position and width for the arctangents and Lorentzians were determined from fits on the Ce L_3 XANES spectra for the CeO_2 and CeF_3 references and on the catalyst taken at ambient conditions. These constraints were then applied to all further fits on the spectra for the reduced catalyst. In this way, from the 16 parameters (4 Lorentzians and 2 arctangents) needed to fit an unknown spectrum only 7 remained as free parameters. The fits on the XANES spectra for the reductions RED1 and RED2 from Figure 12 are given in Figure 14, with indication of the resulting percentages Ce^{3+} and Ce^{4+}. A contribution of about 30% Ce^{3+} is found after each reduction. The absolute error on this concentration determination is estimated to amount to 2-3 percent.

3.2.3. Ce^{4+}/Ce^{3+} evolution during temperature programmed C_3H_8 reduction

The heating of the catalyst from 600 to 763 K in temperature intervals of 8 K (1°/min) in a propane flow of 7.4×10^{-6} mol/s in 3.4×10^{-4} mol/s He at ambient pressure was followed in-situ by taking Ce L_3 spectra with a measuring time of 1 min. For each temperature interval the Ce L_3 XANES spectrum was fitted to obtain the relative Ce^{3+}

and Ce^{4+} concentrations. The amount of Ce^{3+} in the spectra as function of the treatment time and temperature is given in Figure 15. A transition from 0 to about 25% Ce^{3+} in the fit occurs in the 610-640 K temperature interval. After this transition, a further increase in the Ce^{3+} fit percentage as function of time of about 1.3 %/hour can be noticed. Hence, the CuO-CeO_2/Al_2O_3 catalyst presents a clear reduction of the CeO_2 particles during temperature programmed C_3H_8 reduction. This means that not only CuO is reduced by C_3H_8 in this temperature interval, but also CeO_2 to a certain extent.

A clear two-step propane reduction of ceria in the CuO-CeO_2/Al_2O_3 catalyst appears from Figure 15. This two-step process reminds of the bimodal H_2-reduction curve that is characteristic of high surface area ceria [39]. Moreover, a XAS investigation of the H_2-redox properties of ceria in the temperature range of 573 to 773 K has yielded similar observations: for high surface area ceria kept at 673 K, a fast initial H_2-reduction up to about 20% Ce^{3+} was found, followed by a slower reduction [40]. This sequential process for pure ceria was thought to consist of first a fast surface reduction (of outermost Ce^{4+} layers or small particles), followed by slower bulk reduction. The two-step profile is then governed by a balance between reduction kinetics and morphological changes (sintering of ceria into larger particles) [39-40]. For low surface area ceria, only the bulk reduction step is observed [39]. When ceria is supported on alumina, quite different results are being reported regarding H_2-reduction: no reduction below 773 K [5], two reduction peaks at 873 and 1073 K [37] or a single H_2-reduction temperature of 623K has been reported [41].

Even though C_3H_8 and H_2 reduction can only be linked to a certain extent [42], similarities can help identifying the processes that occur. The first transition in the C_3H_8-reduction of Figure 15 occurs in the temperature range 610-640 K. This temperature region can be related to surface reduction of the ceria nanoparticles. The second transition sets off at 640 K and continues with a lower rate up to 763 K. The different slope of both transitions indicates the reduction is dominated by a different mechanism. Given the XRD detection of 7 nm particles, this transition could be related to ceria bulk reduction, which follows a first faster surface reduction. At 763 K the reduction has reached about 32%, but from the constant slope at the end of the temperature range in Figure 15, it can be expected that this reduction process is still incomplete.

The onset of C_3H_8 reduction of ceria in the present catalyst, ~610 K, occurs at quite low temperature, which is similar to the starting reduction of CuO, <623 K (see § 3.1.5).

For CuO-CeO_2/Al_2O_3 catalysts, the presence of CeO_2 is reported to enhance the reducibility of CuO, but most often, H_2-TPR reduction peaks up to 773 K are identified as CuO related only [5, 7, 41]. On the other hand, interaction between CuO and CeO_2 is sometimes believed to enhance the reducibility of both compounds [43]. Such mutual promotion between copper oxide and ceria is then responsible not only for lowering the CuO reduction temperature, but also for inducing a higher ceria reducibility than expected [43]. In the present CuO-CeO_2/Al_2O_3 catalyst system, temperature programmed C_3H_8 reduction induces at first a fast reduction of some 25 % of the Ce^{4+} to Ce^{3+} followed by a slower proceeding reduction. The combined presence of CuO and CeO_2 lowers C_3H_8 reduction temperatures for ceria, so that both compounds start reducing in the same temperature range (≥ 600 K).

4. Conclusions

X-ray absorption spectroscopy was used to follow the C_3H_8 reduction and re-oxidation behaviour of a CuO-CeO_2/Al_2O_3 catalyst, by measuring in-situ both Cu K and Ce L_3 transmission XAS spectra. A detailed analysis including error estimation of the XAS data was performed. The starting material displayed fully oxidized Ce^{4+} and Cu^{2+} and these states were preserved upon pre-treatment (heating to 873 K in He or pre-oxidation at 423 K). From the combined XAS, XRD, XPS and TEM characterisation, it follows that in this CuO-CeO_2/Al_2O_3 catalyst, CuO is present as large single crystallites, while CeO_2 and Al_2O_3 occur as nanoparticles.

Upon reduction with C_3H_8 in the temperature range 600-763 K, Cu^{2+} reduced fully towards metallic Cu^0. QEXAFS was applied to follow this reduction in detail. Analysis of the XANES edge region and a linear combination fit to the EXAFS spectra allowed to identify the presence of some Cu^{1+} during the first stage of the reduction, indicating a two-step reduction process.

In XANES temperature programmed C_3H_8 reduction, Ce was found to partially reduce to Ce^{3+} in two steps: a fast initial reduction up to 25% at low temperature, followed by a slower transition, which continued beyond the investigated temperature range (32% Ce^{3+} at 763 K). The first transition was ascribed to surface reduction of the ceria nanoparticles. The onset temperature of 610 K is similar to the one for the Cu reduction. The second slower reduction is related to bulk reduction of the CeO_2

544 particles. Both processes occur at far lower temperature than expected for bulk ceria,
545 which can only be accounted for by interaction between CuO and CeO_2.
546
547
548 **Acknowledgements**
549 Geert Silversmit is a Postdoctoral Fellow of the Fund for Scientific Research – Flanders
550 (FWO-Vlaanderen). The authors thank the FWO-Vlaanderen for the access to the
551 DUBBLE beam line and financial support. Part of this work was performed in the
552 framework of the Belgian Programme on Interuniversity Poles of Attraction (IUAP V-
553 3) initiated by the Belgian State, Prime Minister's Office, Science Policy Programming.
554 The scientific responsibility is assumed by its authors.
555

References

1. H. Oguchi, T. Nishiguchi, T. Matsumoto, H. Kanai, K. Utani, Y. Matsumura, S. Imamura, Steam reforming of methanol over Cu/CeO_2/ZrO_2 catalysts, Appl. Cat. A: general 281 (2005) 69-73.
2. H. Yahiro, K. Murawaki, K. Saiki, T. Yamamoto, H. Yamaura, Study on the supported Cu-based catalysts for the low-temperature water-gas shift reaction, Cat. Today 126 (2007) 436-440.
3. G. Xie, Z. Liu, Z. Zhu, Q. Liu, J. Ge, Z. Huang, Simultaneous removal of SO2 and NOx from flue gas using a CuO/Al_2O_3 catalyst sorbent I. Deactivation of SCR activity by SO_2 at low temperatures J. Catal. 224 (2004) 36-41 and Simultaneous removal of SO_2 and NO_x from flue gas using a CuO/Al_2O_3 catalyst sorbent II. Promotion of SCR activity by SO_2 at high temperatures J. Catal. 224 (2004) 42-49.
4. P.W Park, J.S. Ledford, The influence of surface structure on the catalytic activity of alumina supported copper oxide catalysts - Oxidation of carbon monoxide and methane, Appl. Cat. B: environmental 15 (1998) 221-231.
5. P.O. Larsson, A. Anderson, Oxides of copper, ceria promoted copper, manganese and copper manganese on Al_2O_3 for the combustion of CO, ethyl acetate and ethanol, Appl. Cat. B: environmental 24 (2000) 175-192.
6. P.O. Larsson, A. Anderson, Complete oxidation of CO, ethanol, and ethyl acetate over copper oxide supported on titania and ceria modified titania, J. Catal. 179 (1998) 72-89.
7. W.P. Dow, Y.P. Wang, T.J. Huang, TPR and XRD studies of yttria-doped ceria/gamma-alumina-supported copper oxide catalyst, Appl. Cat. A: general 190 (2000) 25-34.
8. J.Y. Kim, J.C. Hanson, A.I. Frenkel, P.L. Lee, J.A. Rodriguez, Reaction of CuO with hydrogen studied by using synchrotron-based x-ray diffraction, J. Phys.: Condens. Matter 16 (2004) S3479-S3484.
9. X. Wang, J.C. Hanson, A.I. Frenkel, J.-Y. Kim, J.A. Rodriguez, Interaction of H_2O and NO_2 with BaY faujasite: Complex contraction/expansion behavior of the zeolite unit cell, J. Phys. Chem. B 108 (2004) 13667-13673.
10. H. Oguchi, H. Kanai, K. Utani, Y. Matsumura, S. Imamura, Cu_2O as active species in the steam reforming of methanol by CuO/ZrO_2 catalysts, Appl. Cat. A: General 293 (2005) 64-70.
11. J. Als-Nielsen, G. Grübel, B.S. Clausen, QEXAFS in seconds at an undulator source, Nucl. Instr. Meth. Phys. Res. B 97 (1995) 522-525.
12. A. Caballero, J.J. Morales, A.M. Cordon, J.P. Holgado, J.P. Espinos, A.R. Gonzalez-Elipe, An in situ XAS study of Cu/ZrO2 catalysts under de-NOx reaction conditions, J. Catal 235 (2005) 295-301.
13. A. Yamaguchi, T. Shido, Y. Inada, T. Kogure, K. Asakura, M. Nomura, Y. Iwasawa, In situ time-resolved energy-dispersive XAFS study on the reduction processes of Cu-ZSM-5 catalysts, Bull. Chem. Soc. Jpn. 74 (2001) 801-808.
14. N.R.E Radwan, G.A. Fagal, G.A. El-Shobaky, Effects of CeO2-doping on surface and catalytic properties of CuO/Al_2O_3 solids, Colloids Surfaces A 178 (2001) 277-286.
15. G. Silversmit, M. Olea, H. Poelman, V. Balcaen, P.M. Heynderickx, D. Poelman, R. De Gryse, G.B. Marin, An in-situ XAS study of the structural changes in a CuOCeO2/Al2O3 Catalyst during total oxidation of propane, XAFS13, AIP conference proceedings 882 (2007) 693-695, Editors: B. Hedman, P. Painetta.

16. B.R. Cullity, Elements of X-ray Diffraction, 2nd edition, Addison-Wesley Publishing Company, INC. Reading, Massachusetts, (1978).
17. S. Nikitenko, A. M. Beale, A. M.J. van der Eerden, S. D. M. Jacques, O. Leynaud, M. G. O'Brien, D. Detollenaere, R. Kaptein, B. M. Weckhuysen, W. Bras, Implementation of a combined SAXS/WAXS/QEXAFS set-up for time-resolved in situ experiments, J. Synchrotron Rad. 15 (2008) 632-640.
18. J.-D. Grunwaldt, M. Caravati, S. Hannemann, A. Baiker, X-ray absorption spectroscopy under reaction conditions: suitability of different reaction cells for combined catalyst characterization and time-resolved studies, Phys. Chem. Chem. Phys. 6 (2004) 3037–3047.
19. M. Vaarkamp, J.C. Linders and D.C. Koningsberger, A new method for parametrization of phase-shift and backscattering amplitude, Physica B 208&209, (1995) 159-160.
20. M. Vaarkamp, I. Dring, R.J. Oldman, E.A. Stern, D.C. Koningsberger, Comparison of theoretical methods for the calculation of extended X-ray absorption fine structure, Phys. Rev. B 50 (1994) 7872-7883.
21. J.W. Cook Jr. and D.E. Sayers, Criteria for automatic X-ray absorption fine-structure background removal, J. Appl. Phys. 52 (1981) 5024-5031.
22. D.C. Koningsberger, B.L. Mojet, G.E. van Dorsen, D.E. Ramaker, XAFS spectroscopy; fundamental principles and data analysis ,Topics in Catalysis 10 (2000) 143-155.
23. A.L. Ankudinov, B. Ravel, J.J. Rehr, S.D. Conradson, Real-space multiple-scattering calculation and interpretation of x-ray-absorption near-edge structure, Phys. Rev. B 58 (1998) 7565-7576.
24. F.W. Lytle, D.E. Sayers, E.A. Stern, Report of the international workshop on standards and criteria in X-ray absorption-spectroscopy – March 7-9, 1988 Brookhaven-National-Laboratory , Physica B 158 (1989) 701-722.
25. G.G. Li, F. Bridges, C.H. Booth, X-ray absorption fine-structure standards – a comparison of experiment and theory, Phys. Rev. B 52 (1995) 6332-6348.
26. G. Centi, S. Perathoner, Appl. Cat. A: general 132 (1995) 179-259.
27. M.-F. Luo, P. Fang, M. He, Y.-L. Xie, In situ XRD, Raman, and TPR studies of CuO/Al2O3 catalysts for CO oxidation, J. Mol. Cat. A: Chemical 239 (2005) 243–248.
28. B.R. Strohmeier, D.E. Leyden, R.S. Field, D.M. Hercules, surface spectroscopic Characterization of Cu/Al_2O_3 catalysts, J. Catal. 94 (1985) 514-530.
29. Y. Hu, L. Dong, J. Wang, W. Ding, Y. Chen, Activities of supported copper oxide catalysts in the NO plus CO reaction at low temperatures, J. Mol. Cat. A: Chemical 162 (2000) 307–316.
30. M.M. Günter, B. Bems, R. Schlőgl, T. Ressler, In situ studies on the structure of copper oxide/zinc oxide catalysts, J. Synchrotron Rad. 8 (2001) 619-621.
31. T.L. Reitz, P.L. Lee, K.F. Czaplewski, J.C. Lang, K.E. Popp, H.H. Kung, Time-resolved XANES investigation of CuO/ZnO in the oxidative methanol reforming reaction, J. Catal. 199 (2001) 193-201.
32. Z. Hu, S. Bertram, G. Kaindl, X-ray absorption study of PrO_2 at high-pressure, Phys. Rev. B 49 (1994) 39-43.
33. A. Bianconi, A. Marcelli, H. Dexpert, R. Karnatak, A. Kotani, T. Jo, J. Petiau, Specific intermediate-valence state of insulating 4f-compounds detected by L3 X-ray absorption, Phys. Rev. B 35 (1987) 806-812.
34. A.V. Soldatov, T.S. Ivancheko, S. Della Longa, A. Kotani, Y Iwamoto, A Bianconi, Crystal-strucutre effects in the Ce L(3)-edge X-ray absorption spectrum of CeO2 –

multiple scattering resonances and many-ody final-states Phys. Rev. B 50 (1994) 5074-5080.
35. G. Kaindl, G. Schmiester, E.V. Sampathkumaran, P. Wachter, Pressure-induced changes in LIII X-ray absorption near-edge structure of CeO_2 and CeF_4 – relevance to 4f-electronic structure, Phys Rev. B 38 (1988) 10174-10177.
36. Y. Takahashi, H. Sakami, M. Nomura, Determination of the oxidation state of cerium in rocks by Ce L-III-edge X-ray absorption near-edge structure spectroscopy, Analytica Chimica Acta 468 (2002) 345-354.
37. J.Z. Shyu, W.H. Weber, H.S. Ghandi, Surface characterization of alumina-supported ceria, J. Phys. Chem. 92 (1988) 4964-4970.
38. J.G. Chen, NEXAFS investigations of transition metal oxides, nitrides, carbides, sulfides and other interstitial compounds, Surf. Sci. Reports 30 (1997) 1-152.
39. E. Aneggi, M. Boaro, C. de Leitenburg, G. Dolcetti, A. Trovarelli, Insights into the redox properties of ceria-based oxides and their implications in catalysis, J. Alloys Compd. 408-412 (2006) 1096-1102.
40. J. El Fallah, S. Boujana, H. Dexpert, A. Kiennemann, J. Majerus, O. Touret, F. Villain, F. Le Normand, Redox processes on pure ceria and on Rh/CeO_2 catalyst monitored by X-ray absorption (fast acquisition mode), J. Phys. Chem. 98 (1994) 5522-5533.
41. M., B. Ferrandon, E. Björnbom, F. Klingstedt, A. Kalantar Neyestanaki, H. Karhu, I.J. Väyrynen, Copper oxide-platinum/alumina catalysts for volatile organic compound and carbon monoxide oxidation: Synergetic effect of cerium and lanthanum, J. Catal. 202 (2001) 354-366.
42. K. Chen, A.T. Bell, E. Iglesia, The relationship between the electronic and redox properties of dispersed metal oxides and their turnover rates in oxidative dehydrogenation reactions, J. Catal. 209 (2002) 35-42.
43. X. Tang, B. Zhang, Y. Li, Y. Xu, Q. Xin, W. Shen, CuO/CeO2 catalysts: Redox features and catalytic behaviours, Appl. Cat. A: general 288 (2005) 116-125.

Figure Captions

Figure 1: XRD pattern for the $CuO\text{-}CeO_2/Al_2O_3$ catalyst: A) as received, B) after reduction under propane/He.

Figure 2: STEM images and element mappings of the $CuO\text{-}CeO_2/Al_2O_3$ catalyst, CuO entity in alumina matrix (A); cluster of CeO_2 particles in alumina matrix (B).

Figure 3: Inverted Selective Area Diffractions (SAD) for the $CuO\text{-}CeO_2/Al_2O_3$ catalyst, centred on alumina matrix (A), cluster of CeO_2 particles (B) and CuO entity (C).

Figure 4: Cu K XANES spectra for Cu metal, Cu_2O, CuO and the $CuO\text{-}CeO_2/Al_2O_3$ catalyst taken at ambient temperature.

Figure 5: k^2-weighted EXAFS signals and Fourier Transforms for the $CuO\text{-}CeO_2/Al_2O_3$ catalyst at room temperature and the CuO reference (Catalyst: Δk = 3.47-14.09 $Å^{-1}$; CuO: Δk = 3.55-9.96 $Å^{-1}$).

Figure 6: $k^2*\chi(k)$ and FT[$k^2*\chi(k)$] spectra for the experimental Cu K EXAFS signal of the $CuO\text{-}CeO_2/Al_2O_3$ catalyst at room temperature and the fit (Δk = 3.47-14.09 $Å^{-1}$, ΔR = 0.6-3.3 Å, k^2 variances : 0.66 (Imaginary part) and 0.27 (Absolute part)).

Figure 7: Cu K XANES (left), $k^2*\chi(k)$ and FT[$k^2*\chi(k)$] (right) spectra for the $CuO\text{-}CeO_2/Al_2O_3$ catalyst taken at 723 K, after reduction with C_3H_8/He and for Cu foil at RT in air (Catalyst: Δk = 1.34-12.40 $Å^{-1}$; Cu foil: Δk = 2.07-17.40 $Å^{-1}$).

Figure 8: Fit and experimental $k^3*\chi(k)$ (left) and FT[$k^3*\chi(k)$] (right) spectra for the $CuO\text{-}CeO_2/Al_2O_3$ catalyst after full reduction (Δk = 3.29-10.40 $Å^{-1}$, ΔR = 1.00-5.0 Å, k^3 variances: 0.92 (Imaginary part) and 0.39 (Absolute part)).

Figure 9: Cu K QXANES (left) and QEXAFS (right) spectra for the $CuO-CeO_2/Al_2O_3$ catalyst during propane reduction, 1 minute measuring time per XAS spectrum. The inset shows a detail of the edge structure.

Figure 10: Percentages of Cu^{2+}, Cu^{1+} and Cu^0 contributions to the Cu K QEXAFS spectra of Figure 9 as function of propane reduction time. During the first 3 minutes, the temperature was increased from 423 to 623 K. The error bars represent the 99% confidence intervals from the fitting procedure.

Figure 11: Ce L_3 XANES spectra for the $CuO-CeO_2/Al_2O_3$ catalyst at ambient conditions and the CeO_2, CeF_3 and Ce powder reference compounds.

Figure 12: Ce L_3 XANES spectra for the $CuO-CeO_2/Al_2O_3$ catalyst in a cycle of two subsequent propane reductions with a re-oxidation in between.

Figure 13: Ce L_3 XANES spectra and fits for the CeF_3 (left) and CeO_2 (right) references.

Figure 14: Ce L_3 XANES spectra and fits for the spectra RED1 (left) and RED2 (right) from Figure 12.

Figure 15: Percentage of the CeF_3 spectrum (Ce^{3+} contribution) in the $CuO-CeO_2/Al_2O_3$ Ce L_3 XANES fit as function of reduction time. The temperature increase per step was about 8 K (1 K/min), after an initial heating from 423 to 600 K.

Tables

Table 1: Crystallite sizes determined from XRD in the crushed CuO-CeO_2/Al_2O_3 catalyst as received and after reduction under C_3H_8/He flow at 770 K. An order of magnitude is given for CuO and Cu; averaged values over several diffraction peaks for CeO_2 and Al_2O_3.

crystallite size (nm)	CuO/Cu	CeO_2	Al_2O_3
as received	~ 100	6	4
reduced	~ 100	8	5

Table 2: Specific surface area, nominal ratio Cu/Al and Cu/Ce (from ICP), surface Cu/Al and Cu/Ce ratio and Cu satellite/main peak ratio (from XPS) for the crushed CuO-CeO_2/Al_2O_3 catalyst.

	S_{BET} (m^2/g)	Nominal Cu/Al	Nominal Cu/Ce	Surface Cu/Al	Surface Cu/Ce	Cu_{sat}/Cu_{main}
CuO-CeO_2/Al_2O_3	156	0.10	3.9	0.12	27	0.28

Table 3: Estimated systematic errors in the EXAFS analysis. Error on the Debye-Waller factor (σ^2): 10%.

Absorber – scatterer	systematic error		
	$\lvert\Delta R\rvert$ (Å)	$\lvert\Delta N/N\rvert$ (%)	$\lvert\Delta E_0\rvert$ (eV)
Cu-Cu (1st shell) in Cu metal	<0.018	6	1
Cu-Cu (1st shell) in oxides *N* values from k^2 and k^3 weighted fits only	<0.018	14	<3
Cu-Cu (higher shells)	<0.022	20-30	<3
Cu-O (1st shell)	<0.013	5	1

s

Table 4: Bond distances, *R*, co-ordination numbers, *N*, for the EXAFS fit on the experimental Cu K EXAFS spectrum for the $CuO\text{-}CeO_2/Al_2O_3$ catalyst at room temperature compared to the CuO reference structure values (Δk = 3.47-14.09 $Å^{-1}$, ΔR = 0.6-3.3 Å, k^2 variances: 0.53 (Imaginary part) and 0.23 (Absolute part)).

	Crystal structure		EXAFS fit values			
Absorber - scatter	R (Å)	N	R (Å)	N	σ^2 ($Å^2$)	ΔE_0 (eV)
Cu-O	1.955	2+2	1.938 (±0.022)	6.1 (±1.3)	0.0064 (±0.001)	-0.4 (±1.5)
Cu-O	2.784	2	2.822 (±0.030)	1.0 (±0.5)	0.0064 (±0.001)	-0.2 (±2.4)
Cu-Cu	2.901	4	2.970 (±0.032)	1.6 (±0.3)	0.0029 (±0.001)	-2.7 (±3.6)
Cu-Cu	3.083	4	3.094 (±0.020)	1.5 (±0.3)	0.0029 (±0.001)	-4.6 (±3.2)

Table 5: Comparison between the bond distances *R*, co-ordination numbers *N*, for the Cu K EXAFS fit result on $CuO\text{-}CeO_2/Al_2O_3$ catalyst after full reduction and the fcc Cu crystal structure values (Δk = 3.29-10.40 $Å^{-1}$, ΔR = 1.00-5.0 Å, k^3 variances: 0.92 (Imaginary part) and 0.39 (Real part)).

	Cu fcc crystal structure		EXAFS fit values for $CuO\text{-}CeO_2/Al_2O_3$ catalyst				difference	
Absorber - scatterer	R_{Cu} (Å)	N_{Cu}	R (Å)	N	σ^2 ($Å^2$)	ΔE_0 (eV)	|ΔR| (Å)	N/N_{Cu}
Cu-Cu	2.556	12	2.483 (±0.019)	7.42 (±1.0)	0.019 (±0.003)	5.78 (±1.2)	0.073	0.62
Cu-Cu	3.615	6	3.488 (±0.024)	3.58 (±1.03)	0.019 (±0.003)	10.0 (±3.)	0.127	0.60
Cu-Cu	3.427	24	4.498 (±0.025)	8.02 (±1.7)	0.019 (±0.003)	3.58 (±3.0)	0.071	0.33

Figure01

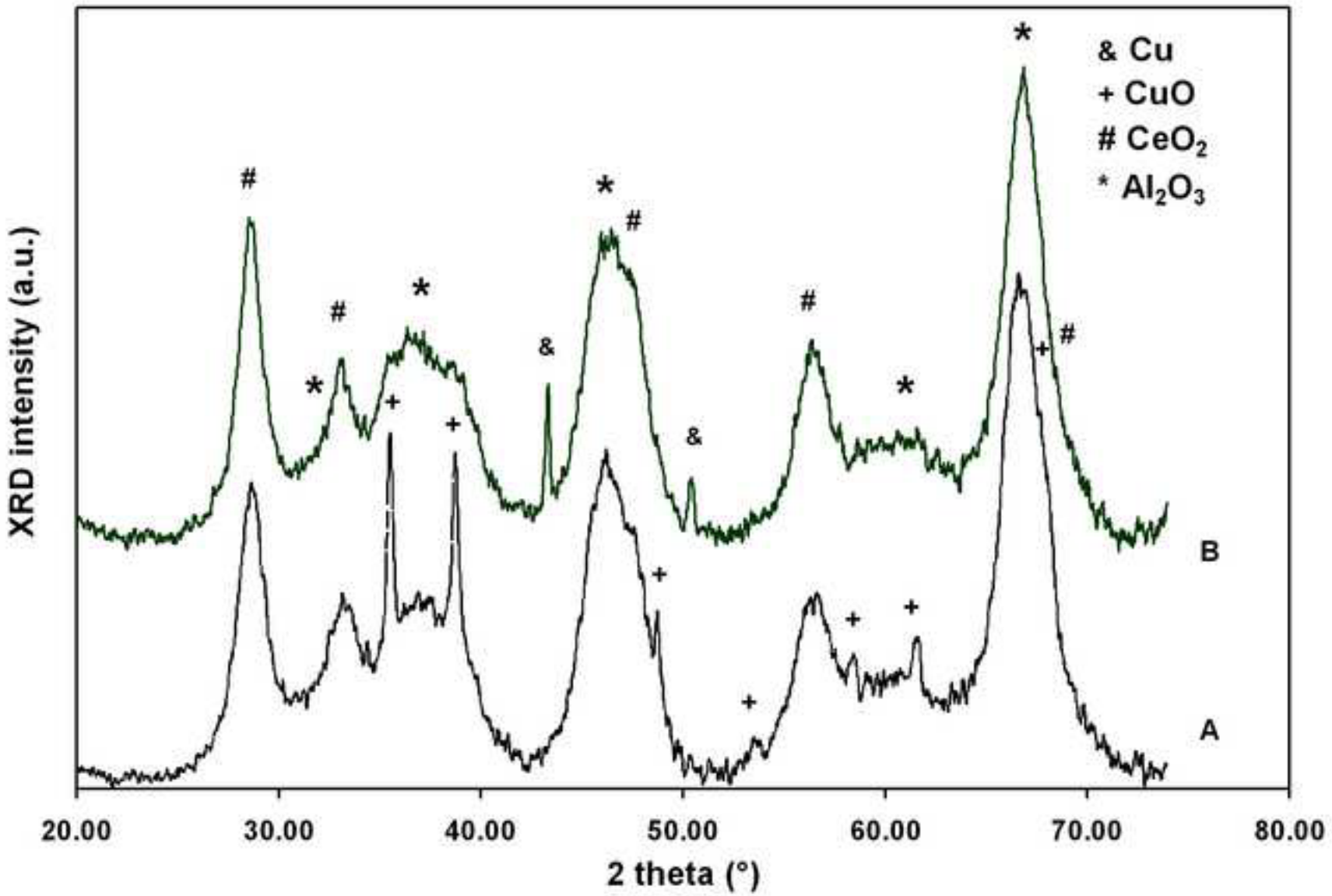

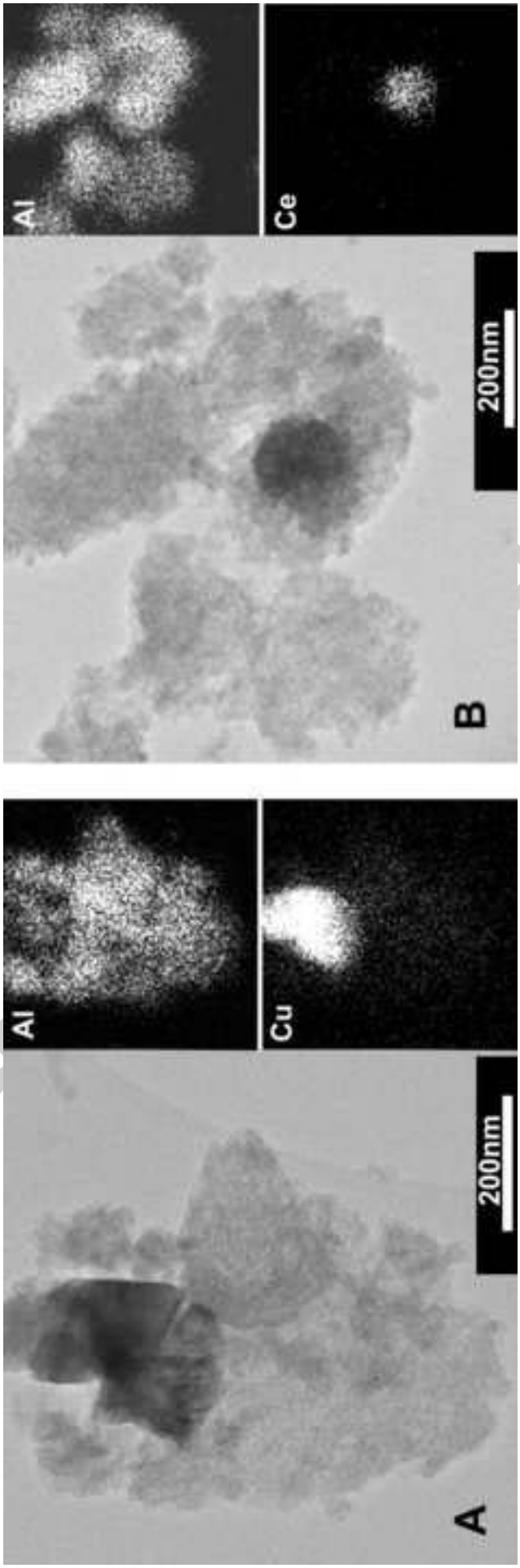

Figure02

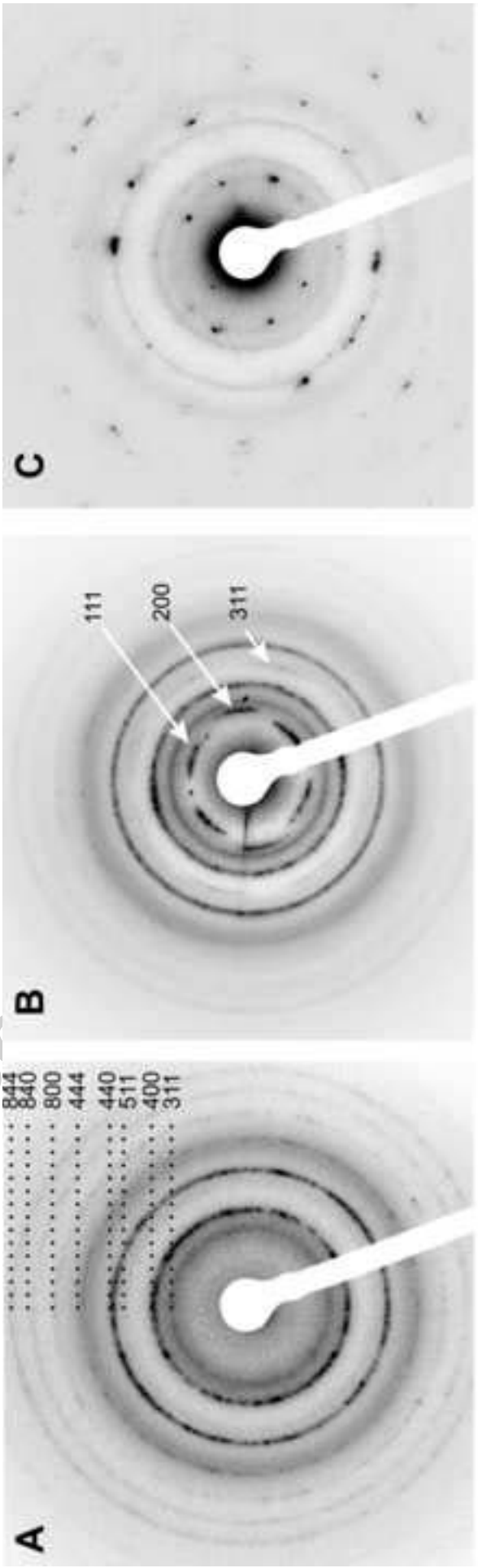

Figure03

Figure04

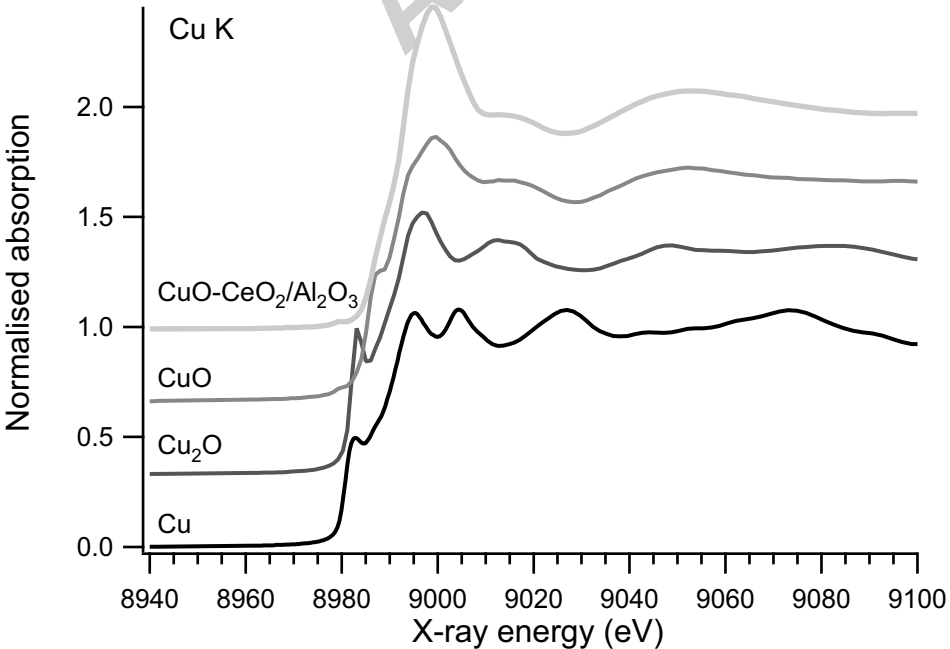

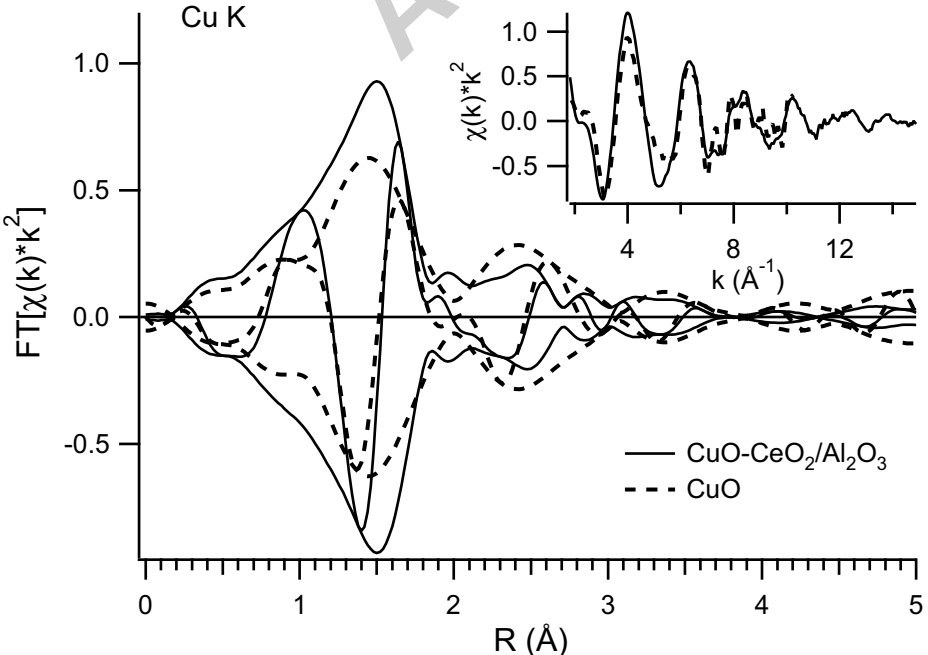

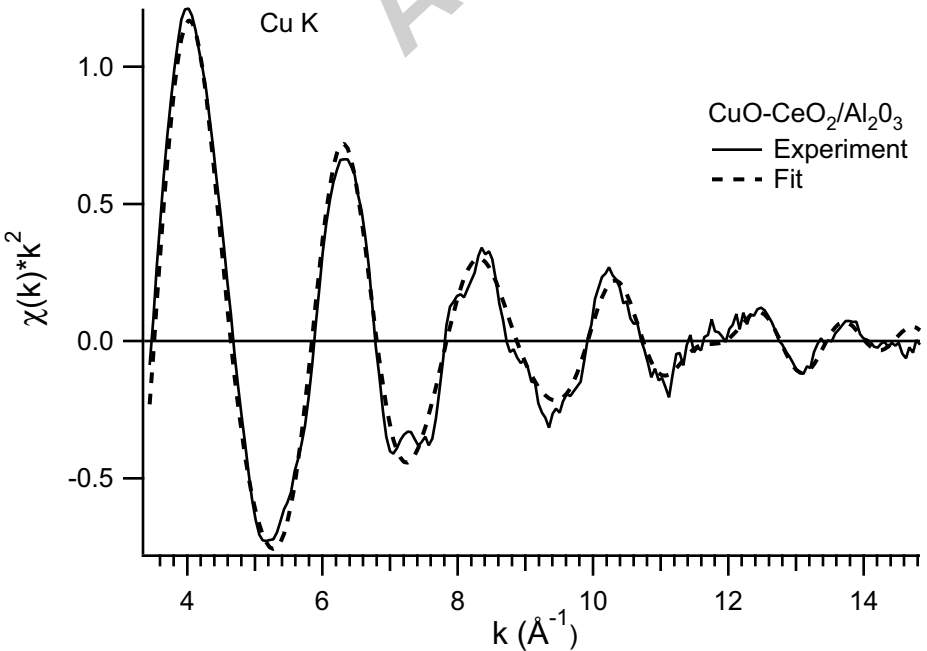

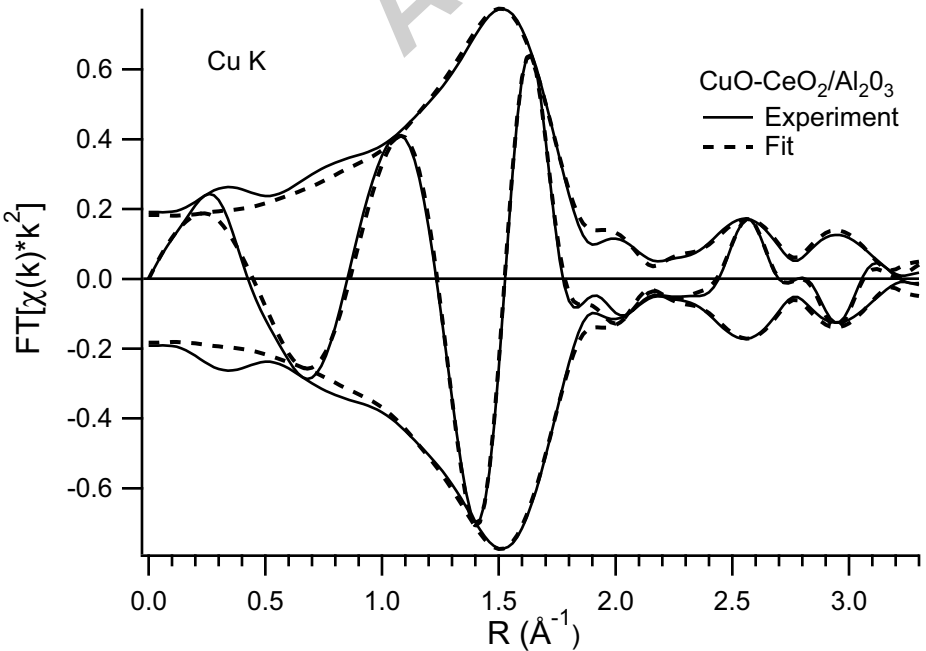

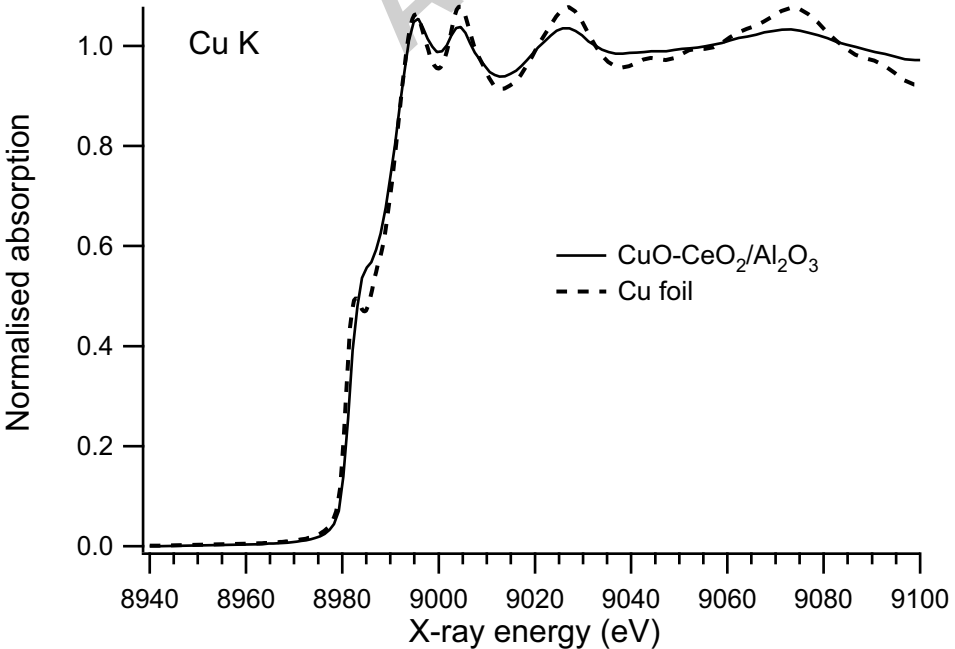

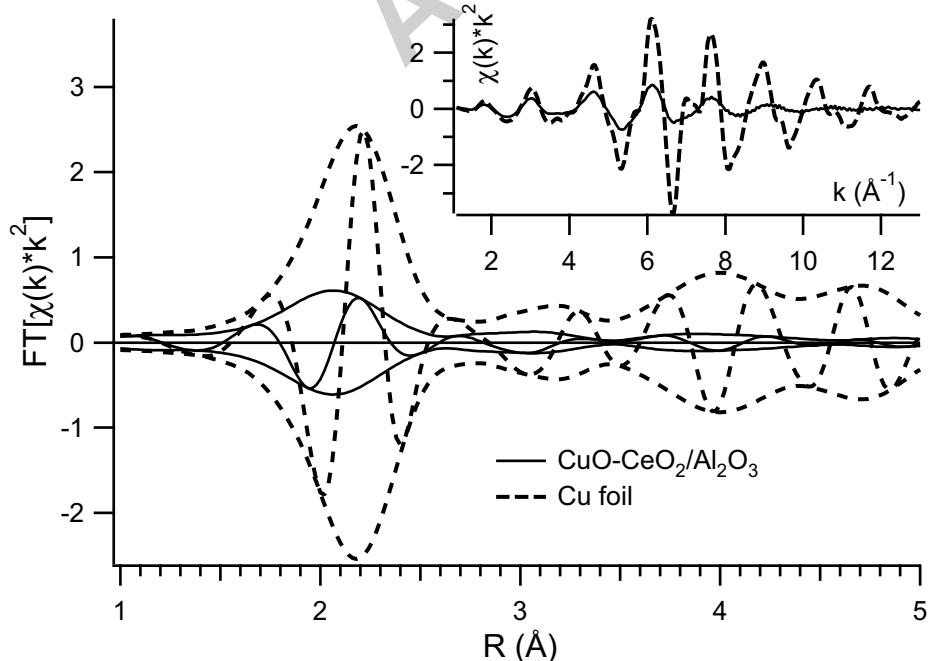

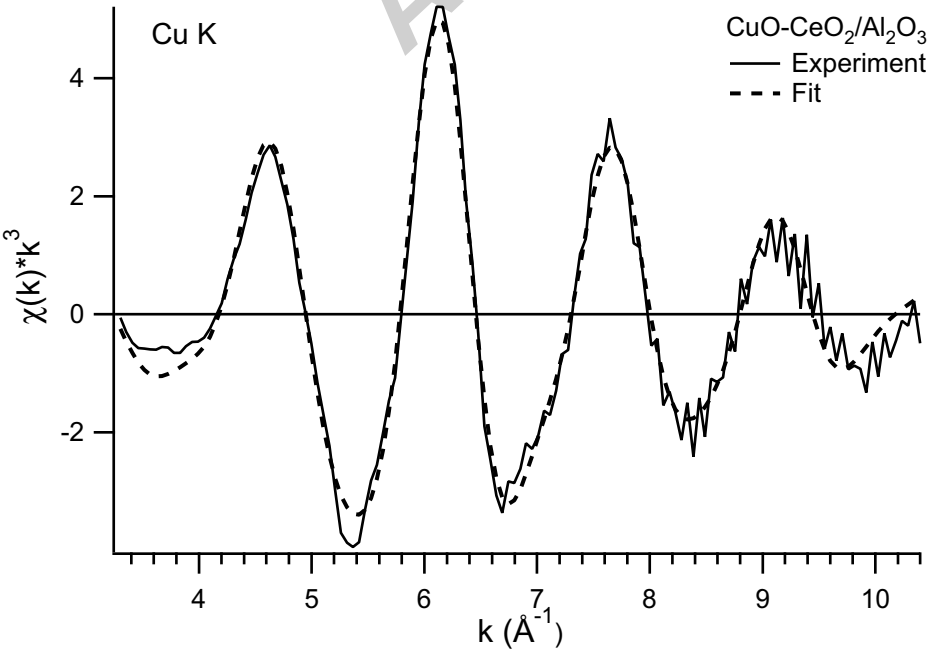

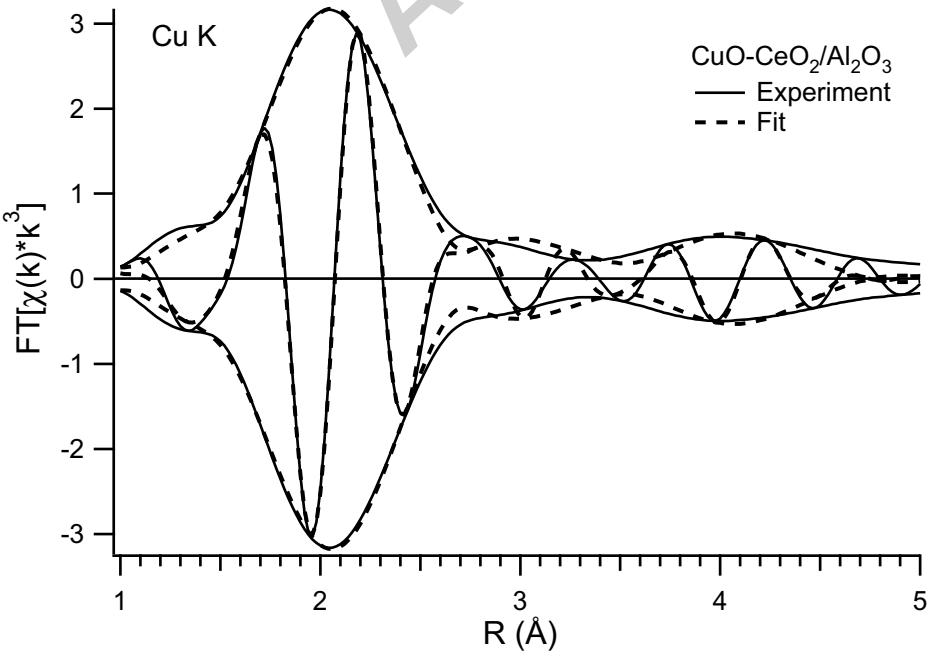

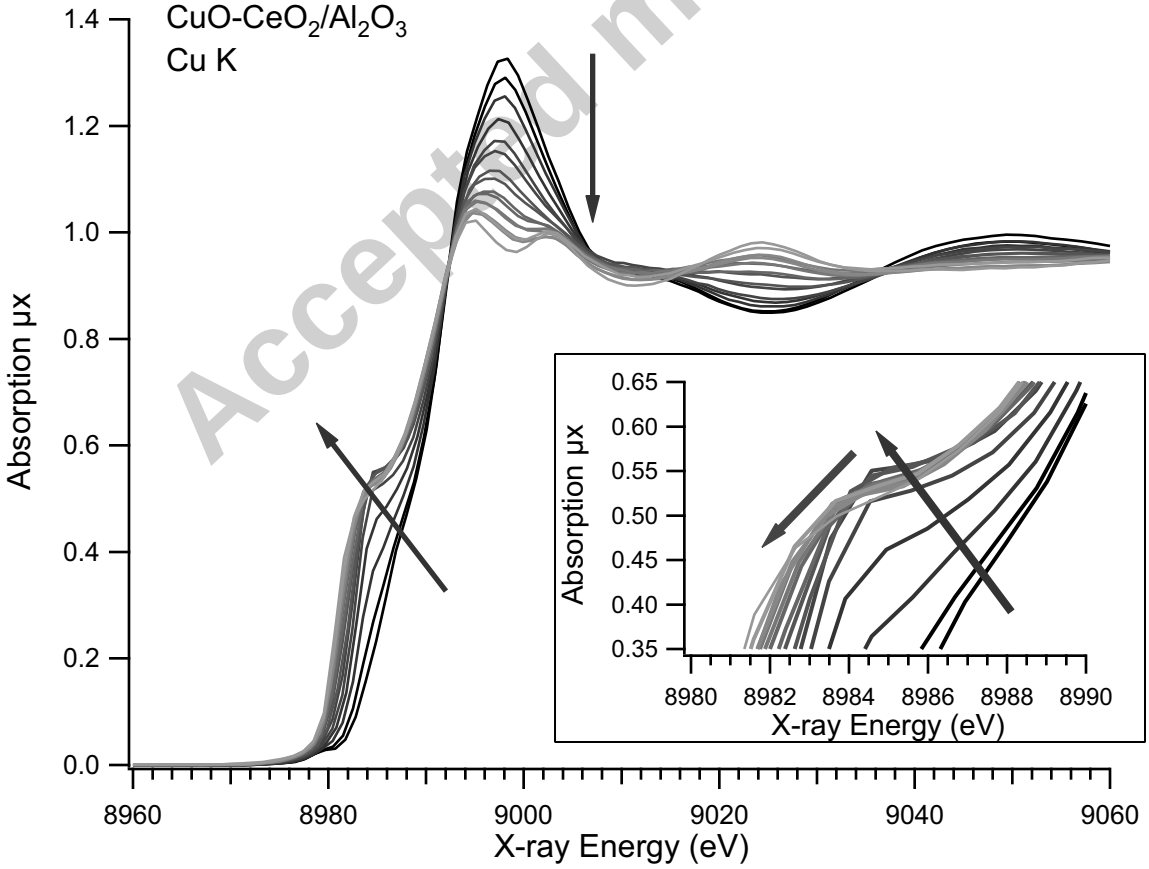

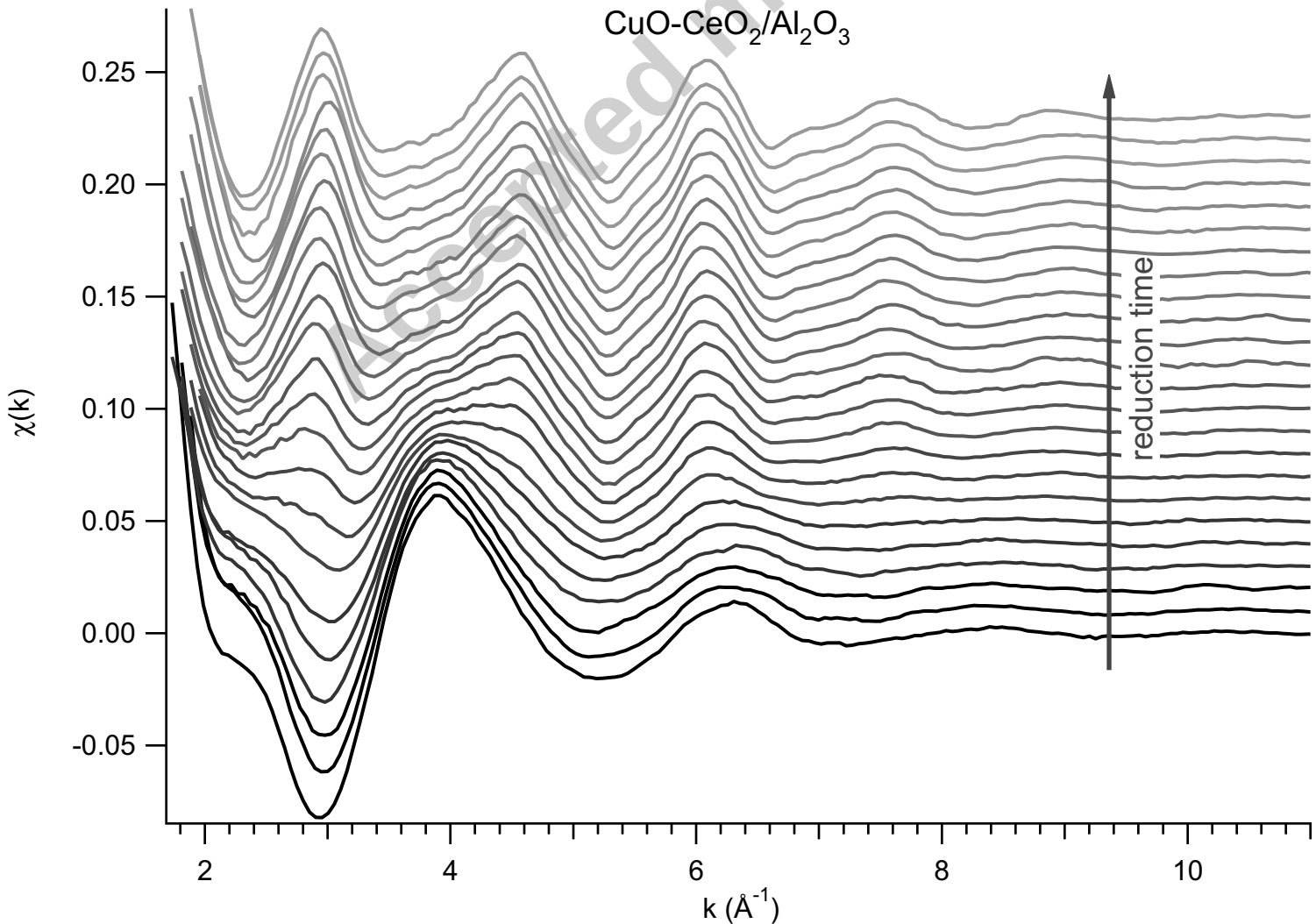

Figure10

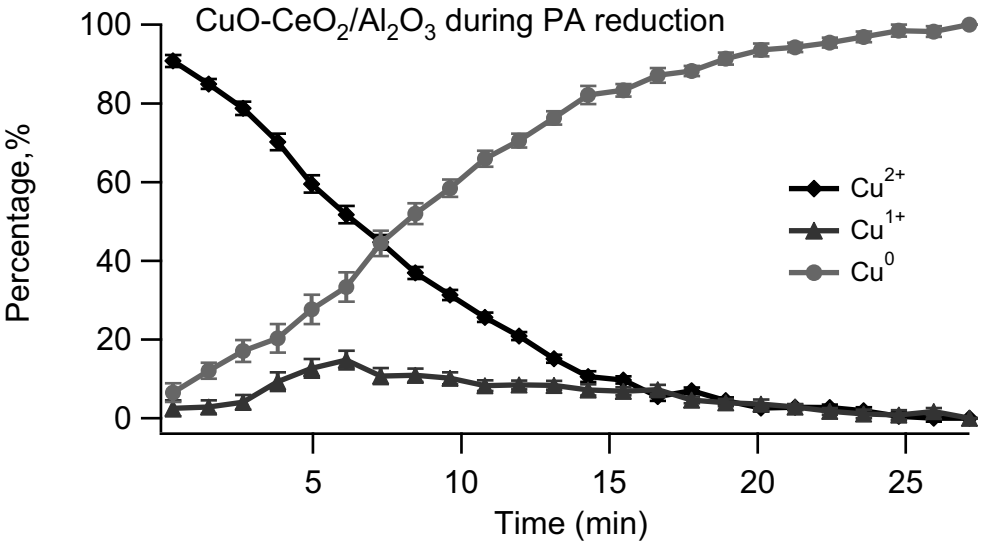

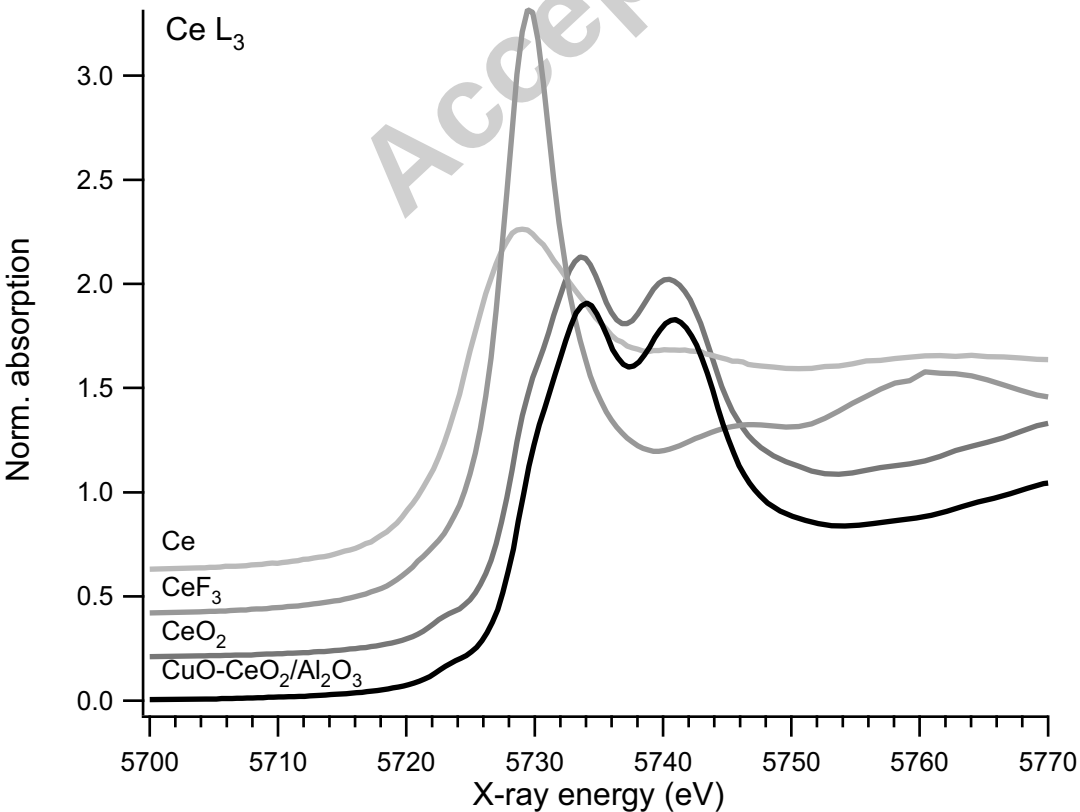

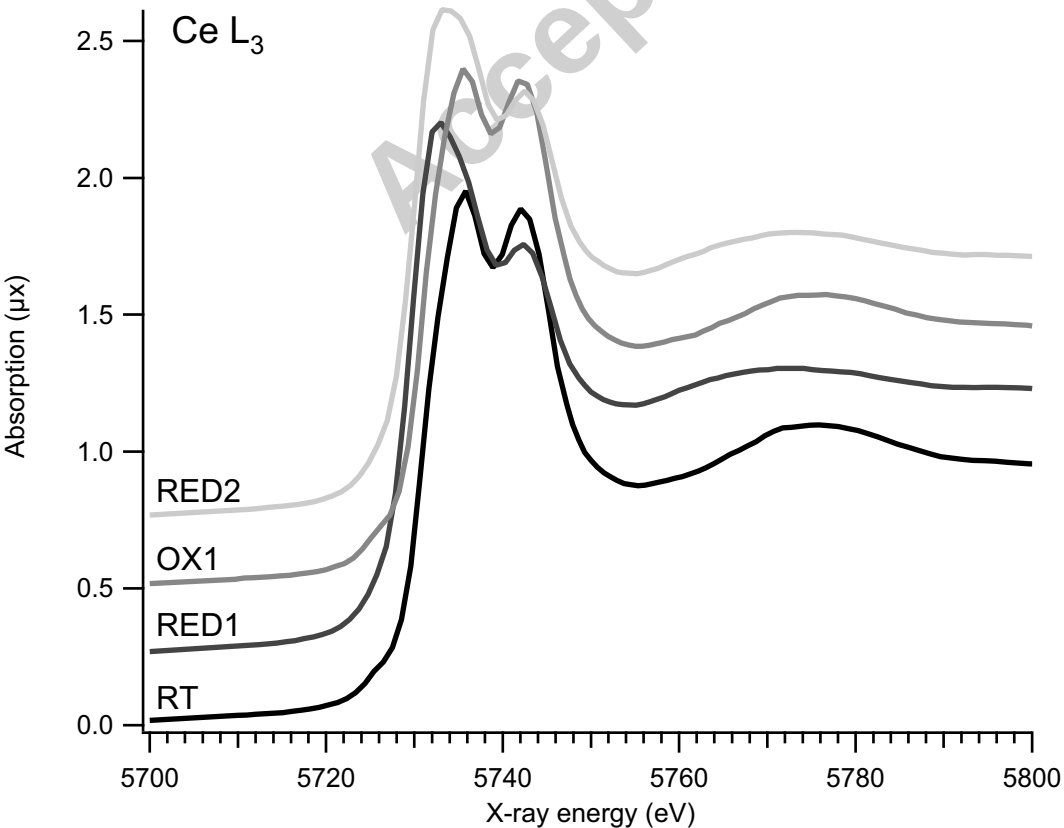

Figure13_left

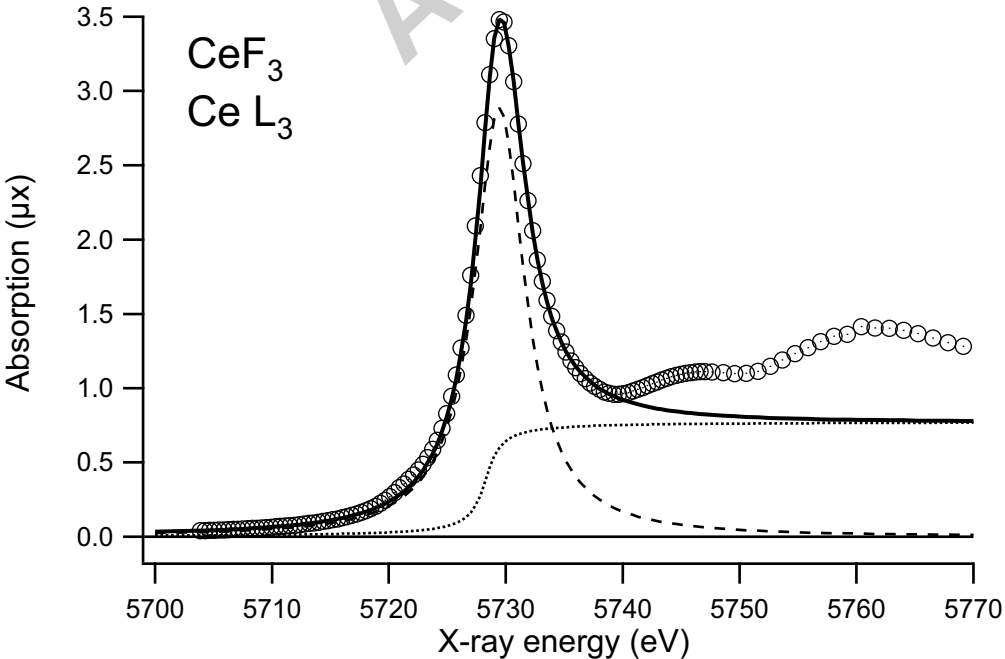

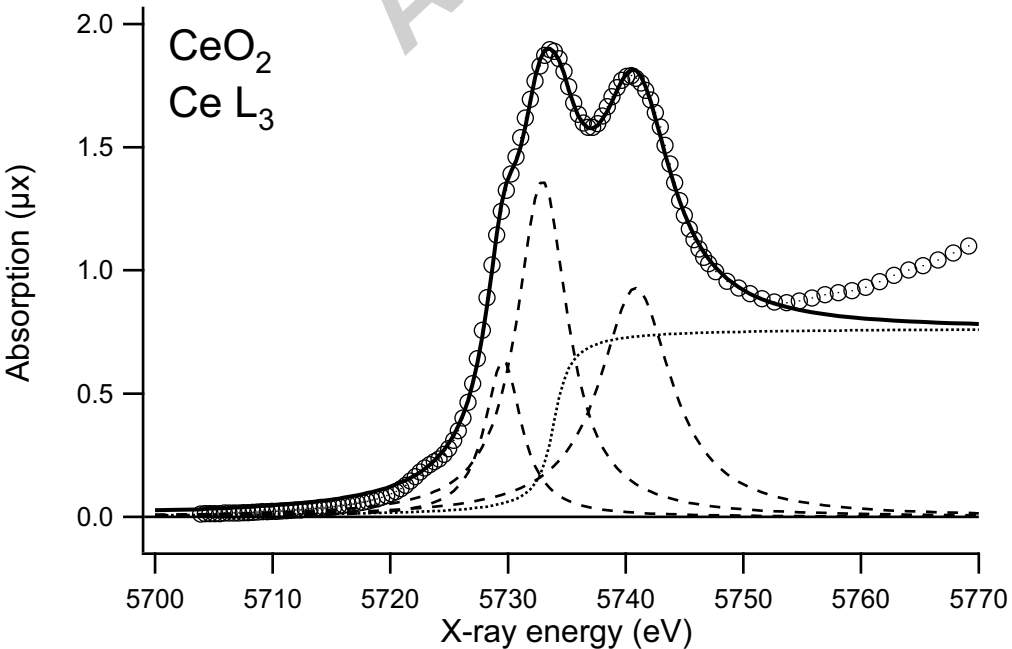

Figure14_left

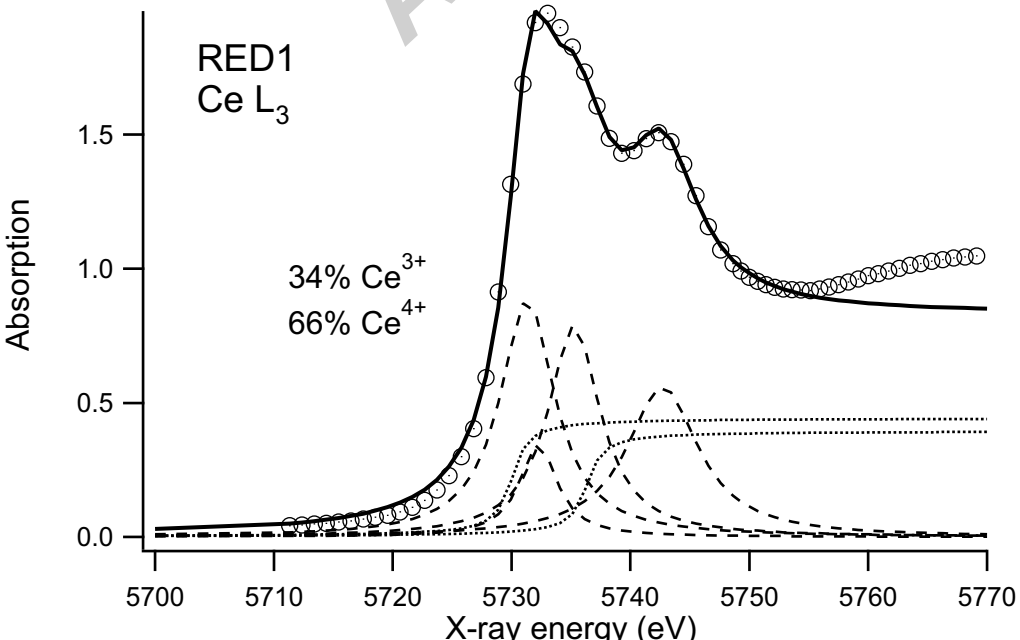

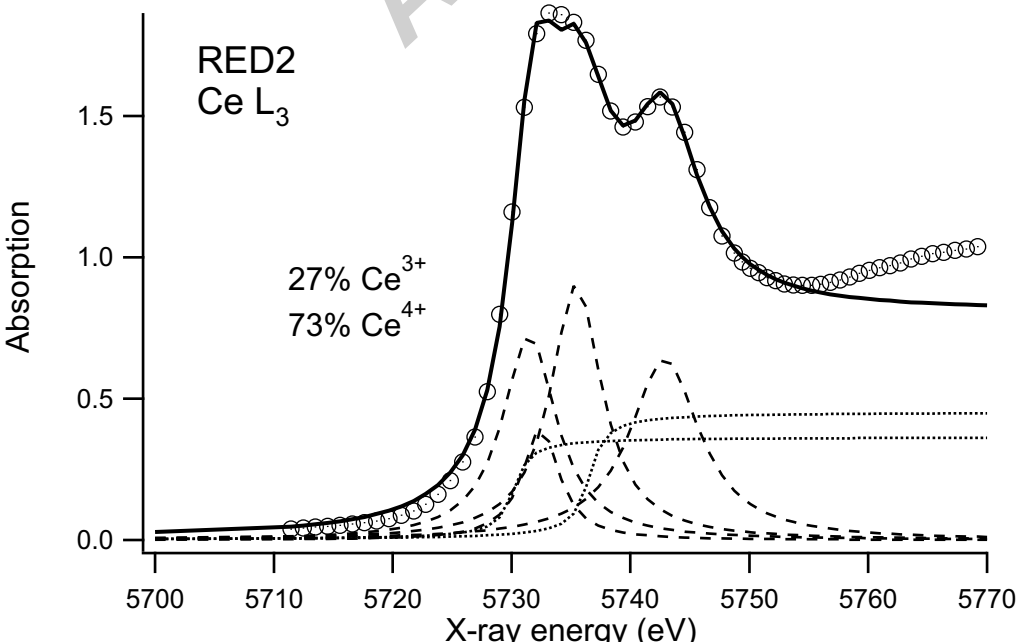

Figure15